Available online at www.sciencedirect.com
SCIENCE DIRECT®
Journal of Computational Physics 196 (2004) 53–87
JOURNAL OF COMPUTATIONAL PHYSICS
www.elsevier.com/locate/jcp

# Sloshing motions in excited tanks

Jannette B. Frandsen *

*Department of Civil and Environmental Engineering, Louisiana State University, Baton Rouge, LA 70803, USA*

Received 17 December 2002; received in revised form 28 October 2003; accepted 28 October 2003

**Abstract**

A fully non-linear finite difference model has been developed based on inviscid flow equations. Numerical experiments of sloshing wave motion are undertaken in a 2-D tank which is moved both horizontally and vertically. Results of liquid sloshing induced by harmonic base excitations are presented for small to steep non-breaking waves. The simulations are limited to a single water depth above the critical depth corresponding to a tank aspect ratio of $h_s/b = 0.5$. The numerical model is valid for any water depth except for small depth when viscous effects would become important. Solutions are limited to steep non-overturning waves. Good agreement for small horizontal forcing amplitude is achieved between the numerical model and second order small perturbation theory. For large horizontal forcing, non-linear effects are captured by the third-order single modal solution and the fully non-linear numerical model. The agreement is in general good, both amplitude and phase. As expected, the third-order compared to the second-order solution is more accurate. This is especially true for resonance, high forcing frequency and mode interaction cases. However, it was found that multimodal approximate forms should be used for the cases in which detuning effects occur due to mode interaction. We present some test cases where detuning effects are evident both for single dominant modes and mode interaction cases. Furthermore, for very steep waves, just before the waves overturn, and for large forcing frequency, a discrepancy in amplitude and phase occurs between the approximate forms and the numerical model. The effects of the simultaneous vertical and horizontal excitations in comparison with the pure horizontal motion and pure vertical motion is examined. It is shown that vertical excitation causes the instability associated with parametric resonance of the combined motion for a certain set of frequencies and amplitudes of the vertical motion while the horizontal motion is related to classical resonance. It is also found that, in addition to the resonant frequency of the pure horizontal excitation, an infinite number of additional resonance frequencies exist due to the combined motion of the tank. The dependence of the non-linear behaviour of the solution on the wave steepness is discussed. It is found that for the present problem, non-linear effects become important when the steepness reaches about 0.1, in agreement with the physical experiments of Abramson [Rep. SP 106, NASA, 1966].


*Keywords:* Sloshing motion; Finite differences; Moving liquid tanks

* Tel.: +1-225-578-0277; fax: +1-225-578-0245.
*E-mail address:* frandsen@lsu.edu (J.B. Frandsen).

0021-9991/$ - see front matter © 2003 Elsevier Inc. All rights reserved.
doi:10.1016/j.jcp.2003.10.031

## 1. Introduction

The present paper investigates numerically steep free surface sloshing in fixed and base-excited rectangular tanks with a focus on moving liquid tanks. Numerical modelling is necessary because neither linear nor second-order potential theory is applicable to steep waves where high-order effects are significant. Recently, Cariou and Casella [6] strengthened this concern through an extensive comparison study of numerical sloshing predictions in ship tanks. The study comprised 11 viscous codes. They concluded and urged the need for further research on accurate free surface predictions.

Prediction of free surface motions of liquids in tanks is of practical importance. Sloshing effects of free-surface motion in tanks driven by external forces may have serious consequences for a range of engineering applications. For example, sloshing effects in the ballast tanks of a ship may cause it to experience large rolling moments, and eventually capsize. Also, if the forcing frequency is near the natural sloshing frequency, the high dynamic pressures due to resonance may damage the tank walls. Further applications in the aerospace industry has been reviewed and discussed comprehensively by Abramson [2], both analytically and experimentally, and recently numerical sloshing motion experiments were carried out by Gerrits [17]. Another example is the use of tuned liquid dampers designed to suppress wind-induced structural vibrations experienced in tall buildings. This type of damping device has been recently installed in a few tall buildings, e.g. the 105 m high Hobart Tower in Tasmania and the 158 m Gold Tower in Japan, as described by Kareem et al. [26]. Designers are faced with the task of understanding complex fluid–structure interactions when attempting to estimate the energy dissipation performance of tuned liquid dampers. To this end, a numerical wave tank can provide useful information on the free surface motions, resonant frequencies, etc.

Sloshing effects in fixed tanks have been the subject of a great deal of past research. For example, Telste [35] modelled inviscid sloshing motion in a 2-D fixed tank by means of a finite difference model. Ferrant and Le Touze [15] applied an inviscid pseudo-spectral model to predict 3-D free sloshing. Ushijima [38] used an arbitrary Lagrangian–Eulerian method on boundary-fitted grids to analyse viscous sloshing and swirling effects in a 3-D cylindrical fixed tank.

There are also several examples of previous studies devoted to investigation of the sloshing waves in moving tanks; both inviscid and viscous formulations. Recently, Bredmose et al. [5] report on "flat-topped" experimentally observed free-surface profiles caused by vertical harmonic forced accelerations. Chen et al. [8] use a finite difference model to examine large sloshing motions in 2-D tanks excited by the horizontal component of four seismic events. For non-overturning waves their model demonstrated that non-linear effects during some earthquakes are responsible for damage of liquid tanks. Chern et al. [9] and Turnbull et al. [37] simulated 2-D forced sloshing in horizontally excited tanks of inviscid liquid (near resonance) using simple $\sigma$-transformed mappings in pseudospectral and finite element schemes. Celebi and Akyildiz [7] developed a viscous solver to capture non-linear free surface flows using the volume of fluid technique, originally developed by Hirt and Nichols [22]. They simulated 2-D sloshing motion in tanks which was forced to roll or to move vertically. Wu et al. [43] use an inviscid finite element model to study the behaviour of non-breaking waves in 3-D tanks. They focus on near resonance cases primarily based on tanks excited by both sway and surge motions and report on the effects of 3-D motions in comparison with 2-D standing waves. Wu et al. show a few tests with pure prescribed heave excitation and one test case included combined sway/surge/heave motions of the tank.

The motivation of the present numerical work is to explore the behaviour of liquid motions in a forced excited tank prescribed to move simultaneously in horizontal and vertical directions. To the author's knowledge, no investigation of the combined motion has been done systematically. Moreover investigators have previously focused on either horizontal or vertical driven excitation. In particular, the vertical tank excitation, as originally explored in Faraday's experiment [14], has had much attention (e.g. the review papers by Miles and Henderson [30]; Perlin and Schultz [32] and the recent work by Jiang et al. [24,25]). The

literature also reveals extensive research on pure horizontal excitation, in general, especially in relation to the application of idealised seismic events [8] and ship stability [10].

Previous numerical models generally treat the moving free surface boundary in one of two ways: either by using Lagrangian tracking of free surface nodes with regridding, or by mappings. The former has the disadvantage that the surface velocities are difficult to predict correctly, and so free surface smoothing is often required. Although mappings inherently overcome this problem, they are less flexible to apply to irregular geometries or to cases where submerged bodies are present in the flow domain. Moreover mapping types of schemes cannot predict run-up/overturning due to the single value formulation [3].

In the present paper numerical experiments of liquid motion in 2-D tanks excited by periodic loadings are undertaken. The fully non-linear numerical model is based on inviscid flow equations and solutions are obtained using finite differences. This paper discusses sloshing motion behaviour in a numerical wave tank based on potential theory mapped according to a modified $\sigma$-transformation that stretches the grid from the bed to the free surface. The $\sigma$-transformation has been widely applied, recently to shallow water flows [27] and to simulate waves in relatively deep water [37]. The present mapping ensures that cell increments have unit dimensions in the discretised mapped domain, and hence simplifies the discretised formulation. The flow equations are solved on a rectangular grid. The sigma-transformation has two major advantages. Remeshing due to the moving free surface is avoided and the mapping avoids the need to calculate the free surface velocity components explicitly. Extrapolations are unnecessary, and so free surface smoothing by means of a spatial filter is often not required. However, it should be noted that the mapping has to be single-valued in the vertical direction, and so the formulation does not permit the free surface to become vertical or overturn. Equivalent solutions on 2-D grid with sigma-transformation are known to be extremely stable, unlike other schemes which have to use free-surface smoothing [37]. Herein complicated free surface behaviour are investigated based on a finite difference scheme which is simple, accurate and computationally efficient. The numerical model is valid for any water depth except for small depth when viscous effects would become important. Moreover, the present model can readily be extended to 3-D waves.

The results presented herein have been limited to a single liquid depth (for reasons of brevity). However, it is very important to note that the liquid depth has a profound influence on non-linear free surface effects. It has been established that there is a critical liquid depth that delineates two non-linear regimes of the liquid free surface referred to as soft and hard spring characteristics. Gu and Sethna [19], Gu et al. [20], Virnig et al. [40] have examined the role of the liquid critical depth in rectangular tanks subjected to vertical sinusoidal excitation. Another important feature is that there is an excitation frequency range over which the free surface exhibits chaotic motion [23]. It should be noted that Ibrahim et al. gives a comprehensive review on sloshing motion predictions with more than 1000 references. The role of critical depth in tanks subjected to horizontal motions have also been studied [10–13,21]. Moreover, Waterhouse [41] investigated liquid behaviour near critical depth and gives a complete fifth-order analysis of soft/hardening spring characteristics.

Analyses of small to steep non-breaking waves are carried out for free and forced sloshing motion in a rectangular tank with constant still water depth providing benchmark tests. The main measure of importance of non-linearity for problems with a free surface is the wave steepness, which for regular waves can be defined as $S = \text{peak-trough/wave length}$. The higher the steepness is, the more important non-linear phenomena become. This may result in interaction between different frequencies or non-linear dispersion effects, as the velocity of wave motion becomes dependent on the amplitude. Usually non-linearity reflects itself through relatively higher peaks and relatively smaller troughs of the surface elevation. The present paper shows results from these free and forced sloshing tests and indicate that the model is capable of simulating highly non-linear free surface motions which is known to occur in steep waves.

First, in Sections 2–4 we present the governing equations, approximate forms and the numerical model. The first test studies are shown in Section 5. Simulations based on fundamental analyses of standing waves in a fixed rigid tank are carried out. The numerical model is validated for different wavelengths. Increasing

wave steepnesses are simulated in order to demonstrate cases where the fully non-linear model provides solutions not obtainable with the approximate forms. In Section 6 the tank is excited vertically and the stability of the sloshing motion is discussed. Benjamin and Ursell [4] investigated the problem theoretically. Their analyses were based on an inviscid flow model with surface tension, and they found that small amplitude wave motion is governed by the Mathieu equation. Benjamin and Ursell concluded that the linearised solutions are always unstable for an external forcing frequency equal to twice the sloshing frequency. The present model investigates the consequences of eliminating the non-linear terms. In Section 7 we focus on the case of pure horizontal tank motion. The solutions for resonant and off-resonant frequency of horizontal excitation for various amplitudes are presented. The influence of non-linearity for high amplitude solutions are illustrated on examples of the surface elevation behaviour, power spectra and phase-plane trajectories. In Section 8 the results are extended for the case of combined horizontal and vertical tank excitation, and emphasis is made on the new flow features generated. It is shown that the vertical tank motion is responsible for the instability of the solution for specific values of motion parameters. In addition to the resonant frequency of the horizontal tank excitation, it is shown that an infinite number of additional resonance frequencies exist due to the combined motion of the tank. The importance of the non-linear effects is discussed for resonant, non-resonant and unstable solutions.

The results presented herein have been computed on a SUN Ultra 60 workstation with 450 MHz CPU (SPECfp95: 32.7). The CPU time required did not exceed 2 h for the fixed tank studies whereas the heave/surge tank tests were the most intensive with an average CPU time of 24 h. Only 12 Mb RAM was required for any test case.

## 2. Governing equations of ideal free-surface waves in moving tanks

Investigations of 2-D non-linear motion of liquid in moving tanks are undertaken. Rectangular tanks which move with respect to an inertial Cartesian coordinate system $(X, Z)$ with horizontal $X$-axis and vertical $Z$-axis, and tank position at time $t$ of $X = X_T(t)$, $Z = Z_T(t)$ are considered. The Cartesian coordinates $(x, z)$ are connected to the tank, with the origin at the mean free-surface at the left-hand side of the tank. The fluid is assumed to be incompressible, irrotational and inviscid. The fluid motion is therefore governed by Laplace's equation,

$$\frac{\partial^2\phi}{\partial x^2} + \frac{\partial^2\phi}{\partial z^2} = 0, \tag{1}$$

where $\phi$ is the velocity potential. In the coordinate system fixed to the tank the fluid velocity components normal to the fixed boundaries are equal to zero. Hence, on the bottom and the walls of the tank we have

$$\left.\frac{\partial\phi}{\partial x}\right|_{x=0,b} = 0; \quad \left.\frac{\partial\phi}{\partial z}\right|_{z=-h_s} = 0, \tag{2}$$

where $b$ is the length of the tank and $h_s$ denotes still water depth. On the free surface the dynamic and kinematic boundary conditions hold, which are

$$\left.\frac{\partial\phi}{\partial t}\right|_{z=\zeta} = -\frac{1}{2}\left[\left(\frac{\partial\phi}{\partial x}\right)^2 + \left(\frac{\partial\phi}{\partial z}\right)^2\right] - (g + Z_T''(t))\zeta - xX_T''(t) \tag{3}$$

and

$$\left.\frac{\partial\zeta}{\partial t}\right|_{z=\zeta} = \frac{\partial\phi}{\partial z} - \frac{\partial\phi}{\partial x}\frac{\partial\zeta}{\partial x}, \tag{4}$$

respectively, where $\zeta$ is the free surface elevation measured vertically above still water level, and $Z''_T$ and $X''_T$ are the vertical and horizontal acceleration of the tank, and $g$ denotes acceleration due to gravity.

Initially the fluid is assumed to be at rest with some initial perturbation of the free-surface. Thus, the initial conditions are:

$$\phi = 0; \quad \zeta = \zeta_0(x) \quad \text{at } t = 0. \tag{5}$$

It should be noted that (5) is difficult to reproduce in a physical experimental treatment because it is not possible to achieve simultaneously $\nabla\phi = 0$ and a non-infinitesimal $\zeta_0$. So it is somewhat hard to imagine that any physical experimental way can generate a single mode in a tank. Nevertheless, understanding the time evolution of the single mode is very important because it can help to predict certain features of the multi-mode forced motion. An example is the vertical excited tank (Section 6) where this ''non-physical'' initial condition is used. Examination of the spectra of the uni-modal motion helps to predict the existence of the side resonances related to for example the combined horizontal/vertical tank motion experiments (Section 8). It is less complicated to deal with non-physical initial conditions in a numerical experimental set-up. The real advantage of numerical methods is the possibility to model situations which are hard to reproduce in physical experiments, but are important from methodological or theoretical view point. But the method of course should be accurate and reliable.

Finally, we should also note that the mean water level in the tank remains constant, that is:

$$\int_0^b \zeta \, \mathrm{d}x = 0. \tag{6}$$

## 3. Approximate solution for sloshing motion in moving tanks

Analytical approaches and related asymptotic solutions to predict sloshing motion in fixed and moving tanks have been explored by several investigators, e.g., Faltinsen et al. [11], Ockendon and Ockendon [31], Hill [21]. Ockendon and Ockendon [31] presents analytical schemes for resonant sloshing due to either vertical or horizontal excitation. They have for example explained mathematically why the schemes require Moiseyev-like detuning and consequently yield a third order secular equation to find the dominant wave amplitude response. Proceeding this way, numerous third-order asymptotic solutions have been derived. For example, Faltinsen [10] derived a third order asymptotic solution for horizontal tank excitation. We should also mention that although Faltinsen et al. [11] present test cases for horizontal tank motions, they have developed a multimodal algorithm for arbitrary tank motions, including roll motion. Hill [21] also investigated transient resonant waves but based on a different third-order analytical algorithm.

As mentioned, the literature reveals that sloshing motion has been investigated with either vertical or horizontal excitation. This section describes an asymptotic solution where combined heave/surge excitations are considered. In the approximations herein, we assume small amplitudes of horizontal motion and initial surface perturbation. The third-order solution presented is limited to single mode resonance cases. We should also mention that our approach is similar to Faltinsen et al. [11] although they use the Hamilton's principle to obtain the evolution equations.

Let us introduce the non-dimensional variables in the following way

$$\phi = \frac{a_c g}{\omega_c}\phi^*; \quad \zeta = a_c\zeta^*; \quad X_T = a_c X_T^*; \quad Z_T = \frac{g}{\omega_c^2} Z_T^*;$$
$$(x, z, b, h_s) = \frac{g}{\omega_c^2}(x, z, b, h_s)^*; \quad t = \omega_c t^*; \quad \omega = \omega^*/\omega_c,$$

where the asterisk is used to denote the non-dimensional values, and $a_c$ and $\omega_c$ are the characteristic wave amplitude and frequency, respectively. Later in this section we shall omit asterisks assuming all the values to be non-dimensional. The choice of the characteristic amplitude and frequency depends on the particular problem in hand and can be related to either the frequency and amplitude of the tank motion or the frequency and amplitude of one of the sloshing modes. The Laplace equation and the surface boundary conditions keep the original forms in the non-dimensional coordinates, while the surface boundary conditions can be rewritten as follows

$$\frac{\partial\phi}{\partial t}+(1+Z_{\mathrm{T}}''(t))\zeta+xX_{\mathrm{T}}''(t)=-\epsilon\frac{1}{2}(\nabla\phi)^2\big|_{z=\epsilon\zeta},\quad \frac{\partial\zeta}{\partial t}-\frac{\partial\phi}{\partial z}=-\epsilon\frac{\partial\phi}{\partial x}\frac{\partial\zeta}{\partial x}\big|_{z=\epsilon\zeta}, \tag{7}$$

where $\epsilon=a_c\omega_c^2/g$ is the characteristic wave steepness. In this section we shall consider the limit of small steepness $\epsilon\to 0$. Expanding the surface boundary conditions into the Tailor series near the mean water level we can rewrite (7) as

$$\begin{aligned}&\frac{\partial\phi}{\partial t}+(1+Z_{\mathrm{T}}''(t))\zeta+xX_{\mathrm{T}}''(t)=-\epsilon\frac{1}{2}\left((\nabla\phi)^2+\zeta\frac{\partial}{\partial t}\frac{\partial\phi}{\partial z}\right)-\epsilon^2\left(\zeta\nabla\phi\nabla\frac{\partial\phi}{\partial z}+\frac{1}{2}\zeta^2\frac{\partial}{\partial t}\frac{\partial^2\phi}{\partial z^2}\right)+\mathrm{O}(\epsilon^3)\Big|_{z=0};\\ &\frac{\partial\zeta}{\partial t}-\frac{\partial\phi}{\partial z}=\epsilon\left(-\frac{\partial\zeta}{\partial x}\frac{\partial\phi}{\partial x}+\zeta\frac{\partial^2\phi}{\partial z^2}\right)+\epsilon^2\left(\frac{1}{2}\zeta^2\frac{\partial^3\phi}{\partial x^3}-\zeta\frac{\partial\zeta}{\partial x}\frac{\partial^2\phi}{\partial x\partial z}\right)+\mathrm{O}(\epsilon^3)\Big|_{z=0}.\end{aligned} \tag{8}$$

The Laplace equation can now be solved in the rectangular domain with the boundary conditions (8) on the mean water level $\zeta=0$.

The general solution of the Laplace equation in the rectangular domain satisfying the boundary condition on the rigid surfaces can be represented in the form of expansion with the linear sloshing modes

$$\phi=\sum_{n=0}^{\infty}\frac{\cosh(nk(z+h_s))}{\cosh(nkh_s)}\cos(nkx)F_n(t);\quad \zeta=\sum_{n=0}^{\infty}\cos(nkx)Z_n(t), \tag{9}$$

where $k=\pi/b$ is the wavenumber corresponding to the first sloshing mode.

The functions $F_n(t)$ and $Z_n(t)$ describing the time evolution of individual components can be found after substituting the general solution (9) into the free-surface boundary conditions (8) and collecting the terms corresponding to different wave numbers $nk$.

First, let us consider the classical perturbation approach. We shall represent the functions $F_n$ and $Z_n$ from (9) in the form of the asymptotic expansion with respect to the powers of the small parameter $\epsilon$

$$F_n=F_n^{(1)}+\epsilon F_n^{(2)}+\cdots;\quad Z_n=Z_n^{(1)}+\epsilon Z_n^{(2)}+\cdots.$$

Substituting into (8) and collecting the terms with the same powers of $\epsilon$ we obtain the equations for each order of approximation. In the main approximation ($\mathrm{O}(\epsilon^0)$) we obtain the following equations describing the linear sloshing of each of the modes

$$F_n^{(1)'}+(1+Z_{\mathrm{T}}'')Z_n^{(1)}=-b_nX_{\mathrm{T}}'';\quad Z_n^{(1)'}-\omega_n^2F_n^{(1)}=0, \tag{10}$$

where $\omega_n=\sqrt{k_n\tanh(k_nh_s)}$ are the linear sloshing frequencies, and $b_n$ are the $n$th coefficients of the Fourier expansion of $x$ with respect to $\cos(nkx)$: $b_0=b/2$, $b_n=0$ for even $n$ and $b_n=-4b/(\pi n)^2$ for odd $n$.

For each component $n$, Eq. (10) can be reduced to a single equation for the surface elevation

$$Z_n^{(1)''}+\omega_n^2(1+Z_{\mathrm{T}}'')Z_n^{(1)}=-b_n\omega_n^2X_{\mathrm{T}}''.$$

In the case of harmonic excitation $X_T(t) = a_h \cos(\omega_h t)$, $Z_T(t) = a_v \cos(\omega_v t)$ this equation can be reduced to the non-homogeneous Mathieu's equation

$$Z_n^{(1)''}(s) + (p - 2q\cos(2s))Z_n^{(1)}(s) = 4b_n\omega_n^2\omega_h^2 a_h \cos(2\omega_h s), \tag{11}$$

where $s = t/2$, $q = 2a_v\omega_v^2\omega_n^2$, $p = 4\omega_n^2$. We note that Eq. (11) represent sloshing motions in a pure vertically excited tank when the right hand side is zero [4].

Solution of the homogeneous Mathieu equation can be represented as a linear combination of two linearly independent Floquet solutions $F_r(z)$, $F_r(-z)$ having the form

$$F_r(z) = e^{irz}P(z),$$

where $r(p,q)$ is the Mathieu characteristic exponent and $P(z)$ is periodic with period $\pi$ [1]. Solution of Mathieu's equation is stable when the value of $r$ is real, and it becomes unstable when the value of $r$ is complex. For small values of the parameter $q$ in the stability regions, the characteristic exponent has the following asymptotic expansion

$$r(p,q) = \sqrt{p} - q^2\frac{1}{4(p-1)\sqrt{p}} - q^4\frac{15p^2 - 35p + 8}{64(p-4)(p-1)^3p^{3/2}} + O(q^6), \tag{12}$$

which can be used to estimate $r$ for small and moderate values of $q$. The contour plots of the real part of the characteristic exponent $r(p,q)$ are represented in Fig. 1, where the thick lines indicate the boundaries of the instability regions.

Furthermore, the function $F_r(z)$ can also be written as a superposition of harmonic oscillations with frequencies $r + 2k$, $k = 0, \pm1, \pm2\ldots$, as follows:

$$F_r(z) = \sum_{k=-\infty}^{\infty} c_{2k}\, e^{i(r+2k)}.$$

If the non-homogeneous Eq. (11) contains solutions in the stable regions, resonance will occur when the frequency of the right hand side equals one of these frequencies. It should be noted, that the strength of

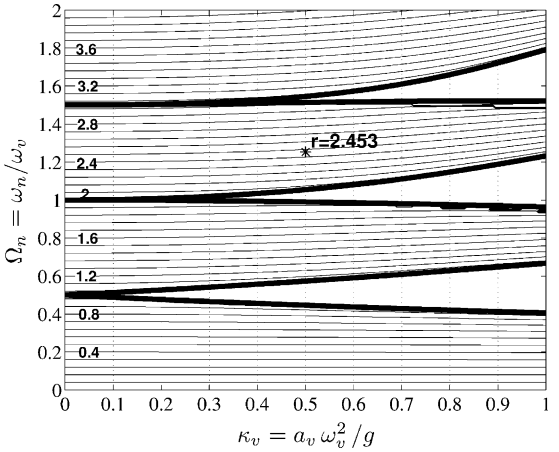


Fig. 1. Stability map for the first-order linear solution including contour plots of Mathieu characteristic exponent $r(4\Omega_n^2, 2\kappa_v\Omega_n^2)$. $r$-values are listed internally on the vertical axis of the figure. The thick lines show the boundaries of instability regions.

these resonances decays faster for large absolute values of $k$. Thus, the first-order solution will exhibit resonant behaviour when the frequency of horizontal excitation $\omega_{\mathrm{h}}$ satisfies the condition

$$\omega_{\mathrm{h}} = \omega_k^{\mathrm{res}} = \frac{r}{2} + k; \quad k = 0, \pm 1, \pm 2, \ldots \tag{13}$$

So in contrast to pure horizontally forced excited tank motion, which exhibits one distinct case of resonance, the case of combined forced tank motion (horizontal and vertical) contains an infinite number of resonances. As it can be seen from (12), for small vertical excitation, as $q \to 0$, the value of $r/2$ goes to $\omega_n$, which in the limit gives the linear resonant frequency for pure horizontal motion.

The right hand sides ($\mathrm{O}(\epsilon^1)$) of the second order equations of Eq. (8) include products of the derivatives of the first-order solutions, which are the infinite sums of sines or cosines. Therefore, for derivations of the second-order solution it is necessary to estimate the $n$th Fourier components of these products. This can be carried out by using the following expression:

$$\sum_{n=0}^{\infty} A_n \cos(k_n x) \sum_{n=0}^{\infty} B_n \cos(k_n x) = \sum_{n=0}^{\infty} C_n(A,B) \cos(k_n x);$$

$$C_n(A,B) = c_n \left( (1 - \operatorname{sign}(n)) A_0 B_0 + A_0 B_n + A_n B_0 + \sum_{j=-\infty}^{\infty} A_{|j|} B_{|n-j|} \right);$$

$$c_0 = \frac{1}{4}; \quad c_n = \frac{1}{2} \quad n = 1, 2, \ldots$$

and

$$\sum_{n=0}^{\infty} A_n \sin(k_n x) \sum_{n=0}^{\infty} B_n \sin(k_n x) = \sum_{n=0}^{\infty} S_n(A,B) \cos(k_n x); \quad S_n(A,B) = \frac{1}{2} \operatorname{sign}(j(j-n)) \sum_{j=-\infty}^{\infty} A_{|j|} B_{|n-j|}.$$

The equations for the time evolution of the second-order Fourier components of the surface elevation and velocity potential can now be written as follows:

$$\begin{aligned} &Z_n^{(2)\prime} - \omega_n^2 F_n^{(2)} = C_n(k^2 F^{(1)}, Z_n^{(1)}) - S_n(kF^{(1)}, kZ^{(1)}), \\ &\Phi_n^{(2)\prime} + (1 + Z_{\mathrm{T}}'') Z_n^{(2)} = -\frac{1}{2} S_n(kF^{(1)}, kF^{(1)}) - \frac{1}{2} C_n(\omega^2 F^{(1)}, \omega^2 F^{(1)}) - C_n(\omega^2 F^{(1)\prime}, Z^{(1)}). \end{aligned} \tag{14}$$

The importance of the cubical non-linearity for the behaviour of dynamical systems is well known [28]. Third order terms can influence the solution in the main approximation leading to an important effect as change of the natural frequency of the system with amplitude. This leads to dramatical changes in behaviour of the non-linear system near resonance compare to a linear one. In the classical perturbation theory such influence can be taken into account, for example, by applying the solvability condition for the third order equations [21] which leads to the restrictions for the behaviour of the first order amplitude. Another way of doing this is to construct a non-linear evolution equation for each of the modes [11]. For high orders the procedure involves extensive algebra including the multiple infinite sums. Nevertheless, in the case when there is one dominating mode, the procedure of constructing an asymptotic solution becomes much simpler. Such a dominating mode will generate only a restricted number of modes in higher orders [10]. This situation, for example, takes place in the case of resonance or instability of one of the modes.

In the case of resonance small horizontal excitation can produce finite perturbations in fluid. We assume that the amplitude of horizontal motion has order $\epsilon^2$. That is

$$X_{\mathrm{T}}(t) = \epsilon^2 \hat{X}_{\mathrm{T}}(t); \quad \hat{X}_{\mathrm{T}}(t) = \mathrm{O}(1) \quad \text{as } \epsilon \to 0.$$

The asymptotic representation of the non-linearly interacting modes is then

$$\phi = \sum_{n=1}^{3} \epsilon^{n-1} \frac{\cosh(nk_m(z+h_s))}{\cosh(nk_m h_s)} \cos(nk_m x) F_{nm}(t); \quad \zeta = \sum_{n=1}^{3} \epsilon^{n-1} \cos(nk_m x) Z_{nm}(t), \tag{15}$$

where $k_m = m\pi/b$ is the wave number corresponding to the dominating mode. The term $n = 0$ is trivial. Because of the constant mean water level we have $Z_0 = 0$, and the corresponding term for the velocity potential is a function of time only and does not produce the contribution into the velocity field. Therefore we have omitted these terms from (15). Substituting (15) into (8) and keeping terms up to $O(\epsilon^2)$, we derive the following non-linear ODE's describing the evolution of the modes in (15)

$$\begin{aligned}
F'_m + (1 + Z''_T)Z_m &= -b_m X''_T + \epsilon^2 \frac{1}{8}\big( -4(2k_m^2 + \omega_m^2\omega_{2m}^2)F_1F_2 - 4\omega_m^2 Z_{2m}F'_m \\
&\quad - 8k_m^2\omega_m^2 Z_m F_m^2 - (3k_m^2 Z_m F'_m + 4\omega_{2m}^2 F_{2m}^2)Z_m\big); \\
F'_{2m} + (1 + Z''_T)Z_{2m} &= \frac{1}{4}(k_m^2 - \omega_m^4)F_m^2 - \frac{1}{2}\omega_m^2 Z_m F'_m; \\
F'_{3m} + (1 + Z''_T)Z_{3m} &= -b_{3m}\hat{X}''_T + \left(k_m^2 - \frac{1}{2}\omega_m^2\omega_{2m}^2\right)F_m F_{2m} - \frac{1}{8}k_m^2 Z_m^2 F'_m - \frac{1}{2}\omega_m^2 Z_{2m}F'_m - \frac{1}{2}\omega_{2m}^2 Z_m F'_{2m}
\end{aligned} \tag{16}$$

and

$$\begin{aligned}
Z'_m - \omega_m^2 F_m &= \epsilon^2\left(Z_m F_{2m} + \left(\frac{1}{8}\omega_m^2 Z_m^2 - \frac{1}{2}Z_{2m}\right)F_m\right); \\
Z'_{2m} - \omega_{2m}^2 F_{2m} &= k_m^2 F_m Z_m; \\
Z'_{3m} - \omega_{3m}^2 F_{3m} &= 3k_m^2 Z_m F_{2m} + \frac{3}{2}k_m^2 Z_{2m}F_m + \frac{3}{8}k_m^2\omega_m^2 Z_m^2 F_m,
\end{aligned} \tag{17}$$

The modes which are not included in (15) do not take part in the non-linear interaction and can be included as independent linear modes. They then satisfy the linear equation (10). In the linear limit, when we neglect all the non-linear terms in (16) and (17), all modes are independent and satisfy Eq. (10).

When considering the particular case studies later in the paper we use specific frequencies and amplitudes as characteristic ones. They are: non-dimensional scale of surface perturbations for single mode motions $\varepsilon = a\omega_n^2/g$, where $a$ is the amplitude of the initial surface perturbation; non-dimensional forcing amplitudes $\kappa_v = a_v\omega_v^2/g$ and $\kappa_h = a_h\omega_h^2/g$, where $a_{v,h}$ and $\omega_{v,h}$ are the amplitudes and frequencies of vertical and horizontal excitations respectively; non-dimensional sloshing frequency $\Omega_n = \omega_n/\omega_v$; width parameters $B = b\omega_v^2/g$, $B_n = b_n/b$; and so on.

## 4. Numerical model

A fully non-linear model for idealised 2-D waves in a numerical wave tank has been developed. A modified $\sigma$-transformation is used to map the liquid domain onto a rectangle, such that the moving free surface in the physical plane becomes a fixed line in the computational mapped domain.

The $\sigma$-transformation was first used by Phillips [33] in connection with numerical weather forecasting schemes. Later the sigma coordinate system was used by Mellor and Blumberg [29] for ocean modeling to improve predictions of both surface Ekman and instabilities in boundary layers. More recently Chern et al. [9] use a Chebyshev expansion to discretise the $\sigma$-transformed potential flow equation in their prediction of

2-D non-linear free-surface motions. The latest model in the literature is described by Turnbull et al. [37] who simulate inviscid free surface wave motions using a 2-D $\sigma$-transformed finite element model.

Fig. 2 illustrates the effect of the mapping in the present model, which has been designed so that each computational cell in the transformed domain is of unit size. This is why we refer to this formulation as the modified $\sigma$-transformation. In this model, remeshing due to the moving free surface is avoided. Other advantages are that the mapping implicitly deals with the free surface motion, and avoids the need to calculate the free surface velocity components explicitly. Extrapolations are unnecessary, and free surface smoothing by means of a spatial filter is not required for the results presented here.

With reference to Fig. 2, the mappings from the physical $(x,z,t)$ domain to the transformed $(X,\sigma,t)$ domain are given by

$$x \leftrightarrow X, \quad X = m_1 + \frac{(m_2 - m_1)}{b}x; \quad z \leftrightarrow \sigma, \quad \sigma = n_1 + \frac{(n_2 - n_1)(z + h_s)}{h}; \quad t \leftrightarrow T, \quad T = t, \tag{18}$$

where $h = \zeta + h_s$; the wave amplitude is $\zeta$, the still water depth is $h_s$, and $b$ is the tank width. We designate the grid size to span from $m_1$ to $m_2$ in the horizontal $x$-direction and $n_1$ to $n_2$ in vertical $z$-direction.

The derivatives of the potential function $\phi(x,z,t)$ are transformed with respect to $x$, $z$ and $t$ into derivatives of $\Phi(X,\sigma,T)$.

The first derivatives of the velocity potential, $\phi$, are obtained as

$$\begin{aligned}
\frac{\partial \phi}{\partial x} &= \frac{(m_2 - m_1)}{b}\left(\frac{\partial \Phi}{\partial X} + \frac{\alpha}{h}\frac{\partial \Phi}{\partial \sigma}\right),\\
\frac{\partial \phi}{\partial z} &= \frac{(n_2 - n_1)}{h}\frac{\partial \Phi}{\partial \sigma},\\
\frac{\partial \phi}{\partial t} &= \frac{\partial \Phi}{\partial T} + \frac{\gamma}{h}\frac{\partial \Phi}{\partial \sigma},
\end{aligned} \tag{19}$$

where $\alpha = -(\sigma - n_1)\frac{\partial \zeta}{\partial X}$ and $\gamma = -(\sigma - n_1)\frac{\partial \zeta}{\partial T}$.

Similarly, Laplace's equation (1) can be rewritten as

$$\frac{\partial^2 \Phi}{\partial X^2} + \frac{1}{h}\left[\frac{\partial \alpha}{\partial X} - \frac{2\alpha}{h}\frac{\partial h}{\partial X}\right]\frac{\partial \Phi}{\partial \sigma} + 2\frac{\alpha}{h}\frac{\partial^2 \Phi}{\partial \sigma \partial X} + \left[\frac{\alpha^2}{h^2} + \frac{b^2(n_2 - n_1)^2}{h^2(m_2 - m_1)^2}\right]\frac{\partial^2 \Phi}{\partial \sigma^2} = 0. \tag{20}$$

The fixed vertical wall boundary condition on $X = m_1, m_2$, and the flat bed boundary condition on $\sigma = n_1$ (2) become

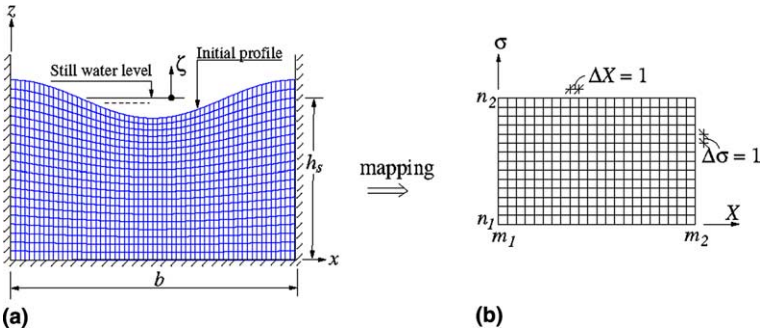


Fig. 2. The physical domain (a) mapped onto the computational domain (b).

$$\frac{\partial \Phi}{\partial X} = -\frac{\alpha}{h}\frac{\partial \Phi}{\partial \sigma}; \quad \frac{(n_2 - n_1)}{h}\frac{\partial \Phi}{\partial \sigma} = 0. \tag{21}$$

The dynamic free-surface boundary condition (3) on $\sigma = n_2$ becomes

$$\frac{\partial \Phi}{\partial T} = \frac{(n_2 - n_1)}{h}\frac{\partial \zeta}{\partial T}\frac{\partial \Phi}{\partial \sigma} - \frac{1}{2}\left[\frac{(m_2 - m_1)^2}{b^2}\left(\frac{\partial \Phi}{\partial X} - \frac{(n_2 - n_1)}{h}\frac{\partial \zeta}{\partial X}\frac{\partial \Phi}{\partial \sigma}\right)^2 + \frac{(n_2 - n_1)^2}{h^2}\left(\frac{\partial \Phi}{\partial \sigma}\right)^2\right] - (g + Z''_{\mathrm{T}})\zeta - \left(\frac{X - m_1}{m_2 - m_1}\right)bX''_{\mathrm{T}}, \tag{22}$$

where $Z''_{\mathrm{T}}$ and $X''_{\mathrm{T}}$ are the vertical and horizontal acceleration of the tank, and $g$ denotes acceleration due to gravity. The kinematic free-surface boundary condition (4) on $\sigma = n_2$ becomes

$$\frac{\partial \zeta}{\partial T} = \frac{(n_2 - n_1)}{h}\frac{\partial \Phi}{\partial \sigma}\left[1 + \frac{(m_2 - m_1)^2}{b^2}\left(\frac{\partial \zeta}{\partial X}\right)^2\right] - \frac{(m_2 - m_1)^2}{b^2}\frac{\partial \zeta}{\partial X}\frac{\partial \Phi}{\partial X}. \tag{23}$$

Eqs. (20)–(23) are then discretised using the second order Adams–Bashforth scheme and solved in the transformed domain iteratively using successive over-relaxation.

The remaining part of the article presents test cases based on the above numerical model. The case studies will report on sloshing motions in fixed, pure vertical and horizontal forced moving tanks. The final study include result of sloshing motion in tanks forced to move simultaneously in horizontal and vertical directions.

## 5. Standing waves in fixed tanks

Simulation of inviscid free sloshing motion in fixed rectangular tanks is the first benchmark validation test which will be presented. The numerical model is validated for different wavelengths. Increasing wave steepness is simulated in order to demonstrate cases where the fully non-linear model provides solutions not obtainable with the approximate forms. Numerical predictions of the free surface motions are compared with analytical results from second-, and third-order potential theory. The entire second order free-surface elevation for the $n$th sloshing mode along the length of the fixed tank can be derived explicitly:

$$\zeta(x,t) = a\left(\cos(\omega_n t)\cos(k_n x) + \frac{a\omega_n^2}{g}\left(\frac{1}{8}\frac{\omega_n^4 + g^2k_n^2}{\omega_n^4} + \left(\frac{1}{8}\frac{3\omega_n^4 - g^2k_n^2}{\omega_n^4} - \frac{3}{2}\frac{\omega_n^4 - g^2k_n^2}{\omega_n^2(4\omega_n^2 - \omega_{2n}^2)}\right)\cos(2\omega_n t) + \frac{1}{2}\frac{\omega_n^2\omega_{2n}^2 - \omega_n^4 - 3g^2k_n^2}{\omega_n^2(4\omega_n^2 - \omega_{2n}^2)}\cos(\omega_{2n}t)\right)\cos(2k_n x)\right), \tag{24}$$

where the linear sloshing frequencies are defined as $\omega_n = \sqrt{gk_n\tanh(k_n h_{\mathrm{s}})}$ and $\omega_{2n} = \sqrt{g2k_n\tanh(2k_n h_{\mathrm{s}})}$. This solution coincides with other investigators [10,42]. The numerical initial conditions which satisfy the velocity potential and free-surface equations are prescribed as

$$\zeta(x,n)|_{t=0} = a\cos(k_n x) \quad \text{and} \quad \phi(x,z)|_{t=0} = 0, \tag{25}$$

where $a$ is the amplitude of the initial wave profile, $k_n = n\pi/b$ is the wave number for $n = 0, 1, 2, \ldots$ and $x$ is the horizontal distance from the left wall.

Non-linear free-surface motions are investigated by varying the initial wave steepness, defined in the fixed tank studies as $\varepsilon = a\omega_n^2/g$, where gravity is $g = 9.81$ m/s$^2$ until near breaking conditions are encountered. The results presented are for a tank of aspect ratio $h_{\mathrm{s}}/b = 0.5$. The linearly stretched grid in the physical domain in accordance with the $\sigma$-transformed Eq. (18) is shown in Fig. 2.

The results herein are based on the first set of numerical tests done by Frandsen and Borthwick [16] who checked the sensitivity of the numerical scheme to the time step and grid resolution. Figs. 3 and 4 illustrate for $n = 1$ and $n = 3$ the time-dependent free surface motion at the wall of the tank for (a) very small amplitude sloshing where $\varepsilon = 0.0014$, and (b) large amplitude sloshing where $\varepsilon = 0.288$. The time histories of the free sloshing analyses are non-dimensionalised with the sloshing frequency $\omega_n$, so that the non-dimensional time $t^* = \omega_n t$, and the non-dimensional time step $\Delta t^* = \omega_n \Delta t$. Although a time step of 0.003 s

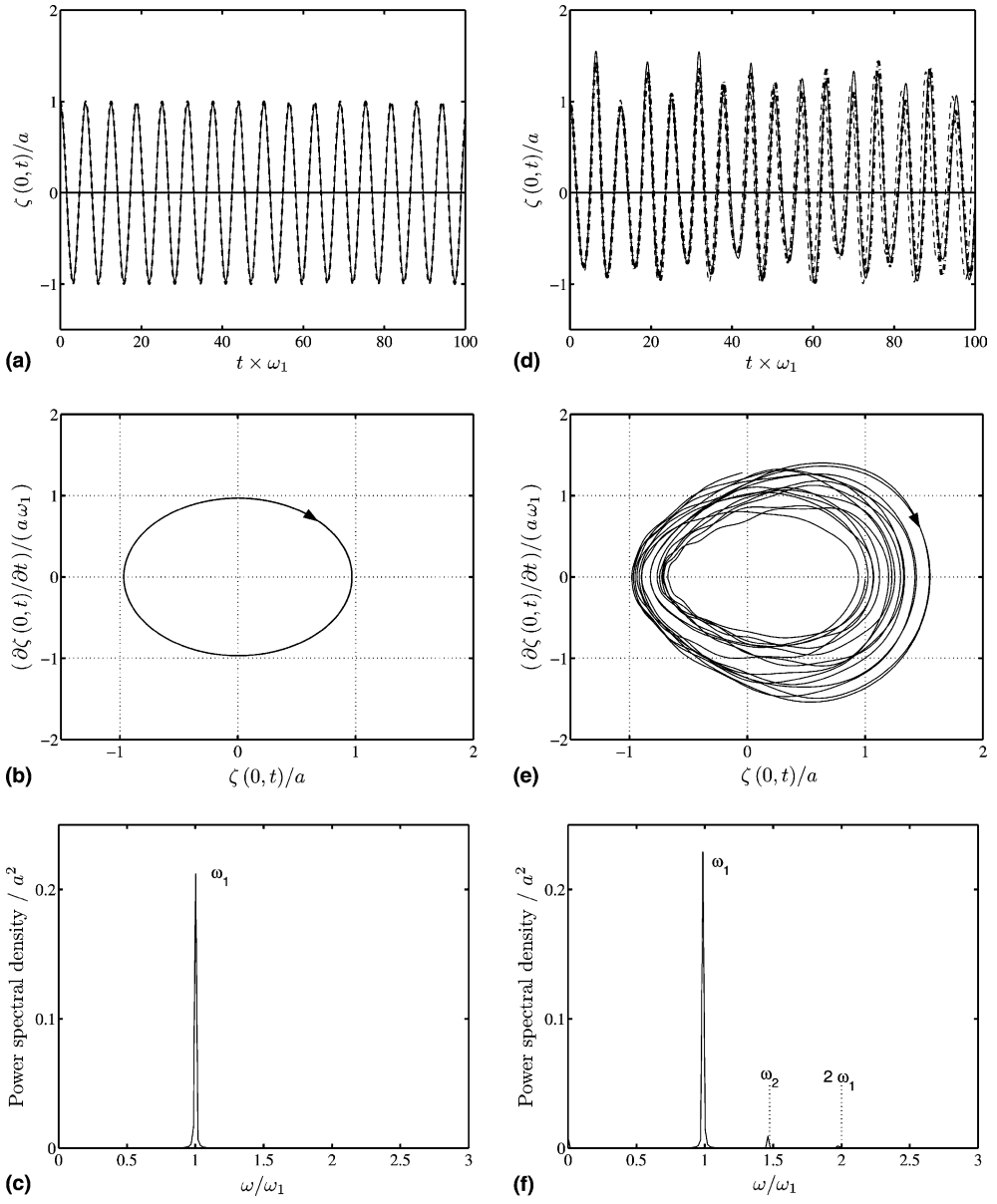


Fig. 3. Free-surface elevation at the left wall in fixed tank for $n = 1$, for (a) $\varepsilon = 0.0014$ and (d) $\varepsilon = 0.288$. - - -, second order solution; - · - ·, third order solution; —, numerical solution. The corresponding wave phase-plane and spectra of the numerical model (b, c) linear solution; (e, f) non-linear solution.

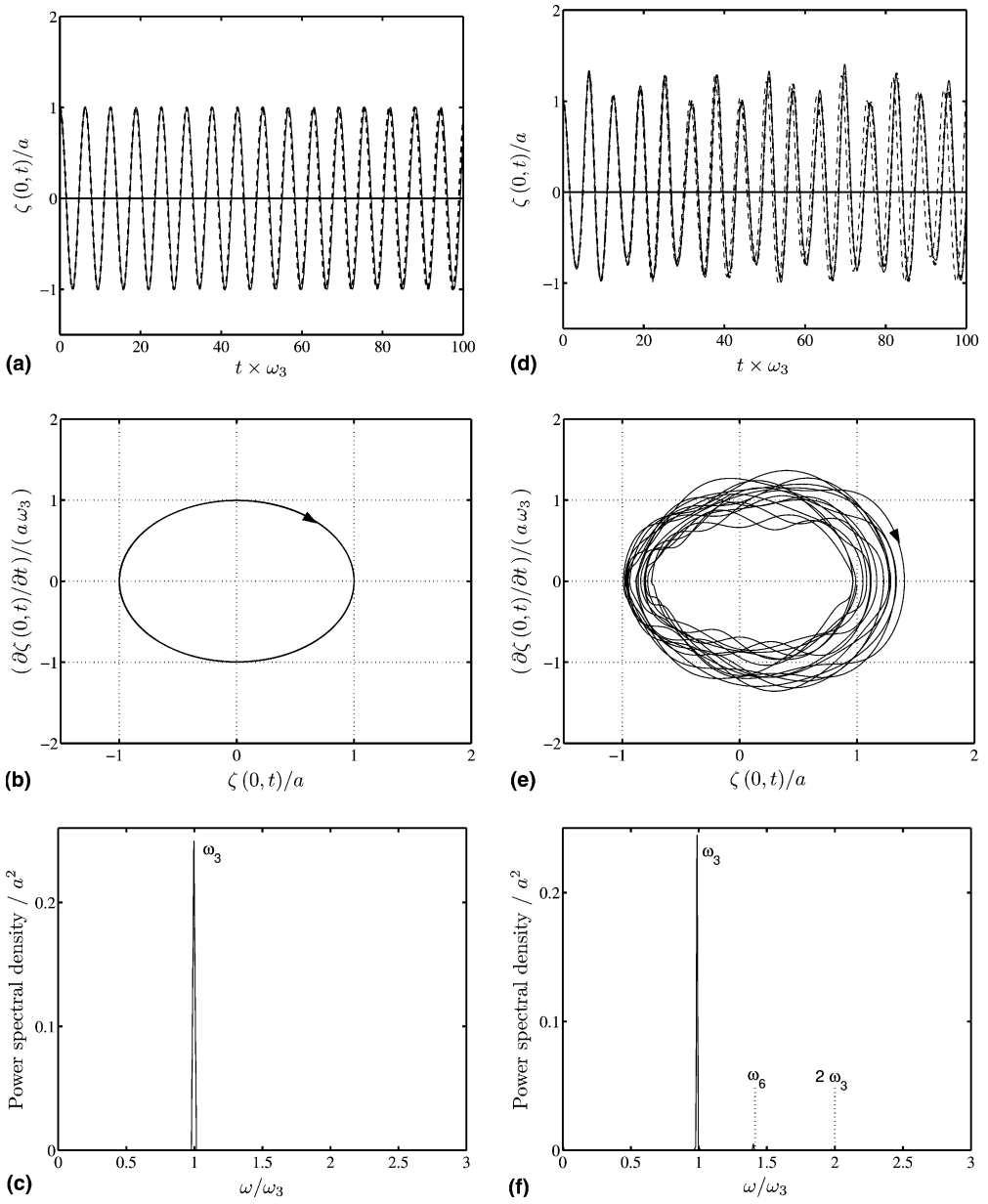


Fig. 4. Free-surface elevation at the left wall in fixed tank for $n = 3$, for (a) $\varepsilon = 0.0014$ and (d) $\varepsilon = 0.288$. - - -, second order solution; - · - ·, third order solution; —, numerical solution. The corresponding wave phase-plane and spectra of the numerical model (b, c) linear solution; (e, f) non-linear solution.

was used in both cases, the grid size was increased in the vertical direction for the larger amplitude test case. A grid size of $40 \times 40$ was sufficient to model accurately small to moderate amplitude waves (approximately $\varepsilon < 0.09$), in comparison with the third-order analytical solution. Increasing the grid points in the vertical direction was found to be more effective in improving accuracy than increasing the grid points in the horizontal direction. A grid size of $40 \times 80$ was used to model steeper waves ($\varepsilon > 0.1$). For large amplitude

sloshing ($n = 1, 3$) it can be observed (Figs. 3(d) and 4(d)) that the phase-shift grows in time between the second order analytical solution and the fully non-linear numerical model. The maximum amplitudes are also higher than those of the approximate solution. This has also been observed by Tadjbakhsh and Keller [34], Vanden-Broeck and Schwartz [39], Tsai and Jeng [36] and Greaves et al. [18]. The third order approximate solution compares well with the numerical solution with regard to the phase. The third-order solution, however, tends to underpredict the peaks and overestimate the through, especially when the numerical predicted trough are smallest. The peaks following the smallest trough are also not captured well by the third order solution. This effect is more evident for $n = 1$ than $n = 3$ due higher non-linearity.

The influence of non-linearity can be seen more clearly on the phase-plane diagrams in Figs. 3(b), (e) and 4(b), (e). The small amplitude diagrams (b) display linear behaviour of the free surface with repeatable patterns for the peaks and troughs in bounded orbits, while the large amplitude cases (e) show bounded solutions with higher peaks caused by non-linearity.

Figs. 3(c), (f) and 4(c), (f) show the associated spectra. The spectra of small amplitude waves (c) display the fundamental sloshing frequency. It can be observed that small additional frequencies due to non-linear mode to mode interaction are present for the large initial amplitude cases (f). We note that they are responsible for the large disturbances in the free surface elevation.

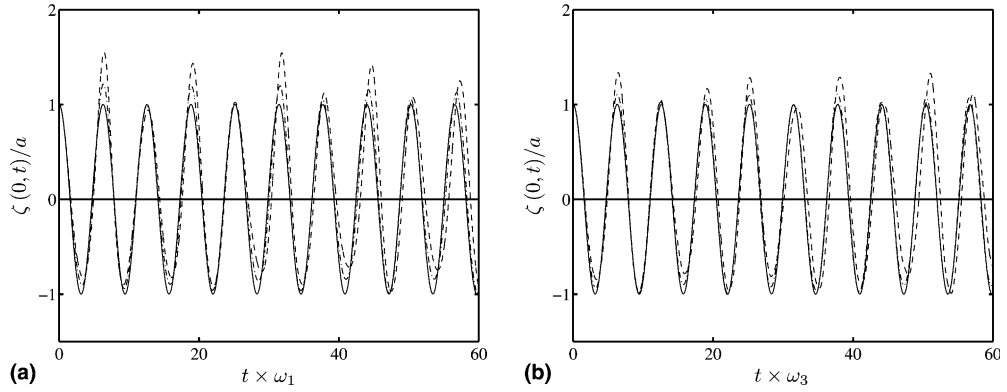


Fig. 5. Free-surface elevation at the left wall in fixed tank for wave steepness of —, $\varepsilon = 0.0014$; - · -, $\varepsilon = 0.144$; - - -, $\varepsilon = 0.288$; for (a) $n = 1$ and (b) $n = 3$.

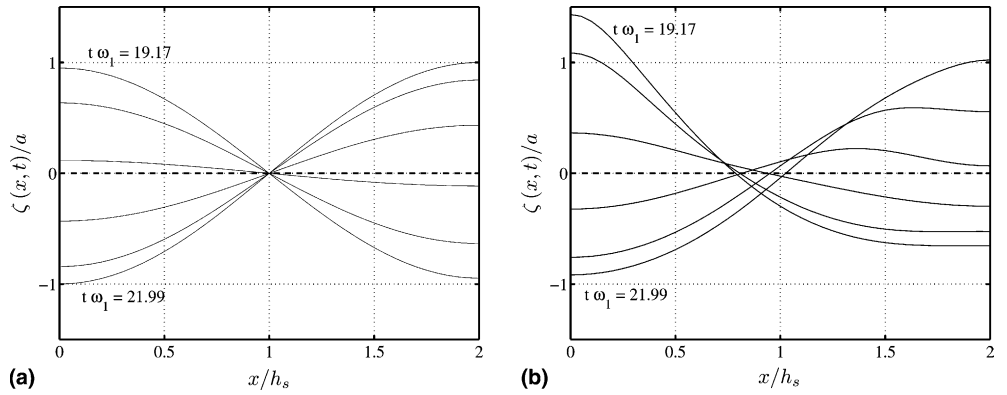


Fig. 6. Wave profiles for a typical half-period, $n = 1$, for (a) $\varepsilon = 0.0014$ and (b) $\varepsilon = 0.288$.

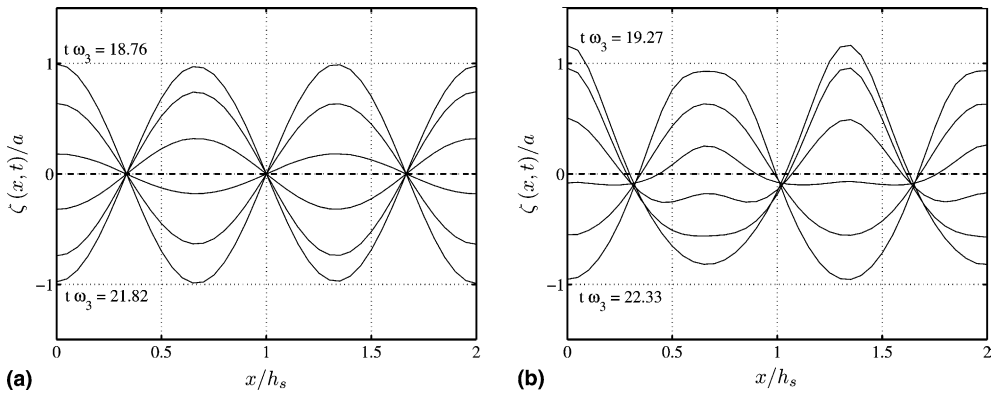


Fig. 7. Wave profiles for a typical half-period, $n = 3$, for (a) $\varepsilon = 0.0014$ and (b) $\varepsilon = 0.288$.

Fig. 5 shows the effect of increasing wave steepness on the free surface time history at the tank wall. As expected, the wave motions become progressively non-linear as the steepness increases. This is reflected by the higher peaks, lower troughs with a growing phase-shift, as time evolves.

Furthermore, the corresponding numerical wave profiles across the tank at different times during a typical sloshing period for $n = 1$, 3 are also shown in Figs. 6 and 7. The small amplitude waves (a) display linear standing waves whereas the steep wave cases (b) exhibit a dispersion effect that is most evident at the nodes. Other $\sigma$-methods show identical behaviour as reported by other investigators [9,37].

## 6. Vertically excited tanks

The second set of validation tests is concerned with forced sloshing of liquid in a rectangular tank subjected to vertical base-excitation.

The coordinate system of the numerical model is fixed at the left wall of the tank, and moves with the tank. The only change to the governing Eqs. (20)–(23) of the numerical model is the dynamical free-surface boundary condition (22) in which $X''_{\mathrm{T}} = 0$. The tank is assumed periodically excited with the vertical base acceleration, $Z''_{\mathrm{T}} = -\omega_{\mathrm{v}}^2 a_{\mathrm{v}} \cos(\omega_{\mathrm{v}} t)$, where $a_{\mathrm{v}}$ is the vertical forcing amplitude, $t$ is time and $\omega_{\mathrm{v}}$ is the angular frequency of forced vertical motion. The initial conditions are equivalent to the sloshing motion simulation in a fixed tank (25). In the vertically excited tank test cases the parameter $\kappa_{\mathrm{v}} = a_{\mathrm{v}}\omega_{\mathrm{v}}^2/g$ is a measure of the importance of the vertical forcing motion and $\varepsilon$ is a measure of non-linearity. Numerical predictions of the free surface motions are compared with analytical results from second-, and third-order potential theory. First we note that the linear solution for the motion of fluid in a vertically excited tank was first obtained by Benjamin and Ursell [4], who also investigated the stability of this motion. In the case when the initial surface perturbation includes only one Fourier component $\zeta(0, x) = a\cos(k_n x)$ the solution does not includes infinite sums and can be represented in a relatively simple form. The second-order correction for the surface elevation then consist only of the double wavelength term and the entire second order solution can be written explicitly as

$$\zeta(x,t) = a\cos(k_n x) Z_n^{(1)}(\omega_{\mathrm{v}} t) + a\left(\frac{a\omega_{\mathrm{v}}^2}{g}\right)\cos(k_{2n} x) Z_{2n}^{(2)}(\omega_{\mathrm{v}} t), \tag{26}$$

where the amplitude of the initial perturbation ($a$) is used as a characteristic amplitude of the wave. The first and second-order evolution functions $Z_{n,2n}^{(1,2)}$ satisfy the homogeneous and non-homogeneous Mathieu equations:

$$Z_n^{(1)''}(\omega_v t) + \Omega_n^2(1 + \kappa_v V''(\omega_v t))Z_n^{(1)}(\omega_v t) = 0;$$

$$Z_{2n}^{(2)''}(\omega_v t) + \Omega_{2n}^2(1 + \kappa_v V''(\omega_v t))Z_{2n}^{(2)}(\omega_v t) = \frac{1}{2\Omega_n^2}\left(\left(\frac{1}{2}\frac{\Omega_{2n}^2}{\Omega_n^2} + 2\right)\frac{K_n^2}{B^2} - \frac{\Omega_n^2\Omega_{2n}^2}{2}\right)Z_n^{(1)'}(\omega_v t)^2 - (1 + \kappa_v V''(\omega_v t))\left(\frac{K_n^2}{B^2} - \frac{\Omega_n^2\Omega_{2n}^2}{2}\right)Z_n^{(1)}(\omega_v t)^2,$$

where $B = b\omega_v^2/g$, $\Omega = \omega_n/\omega_v$, $K = \pi n$, and with the following non-dimensional initial conditions

$$Z_n^{(1)}(0) = 1; \quad Z_{2n}^{(2)}(0) = 0; \quad Z_n^{(1)'}(0) = Z_{2n}^{(2)'}(0) = 0.$$

The free surface motions are examined in cases of increasing wave steepnesses, inside and outside of the regions of parametric resonance (instability regions). The six test cases considered herein are marked on the stability map in Fig. 8. The results presented are for a tank of aspect ratio $h_s/b = 0.5$.

The first set of tests are carried out in a stable zone, with frequency ratio $\Omega_1 = 1.253$, and a non-dimensional forcing amplitude, $\kappa_v = 0.5$. The time histories for the free surface elevation for small and high wave steepnesses are shown in Fig. 9. Good agreement between the approximate solution and the numerical model is achieved for small amplitude waves. The behaviour of the free surface motion in the vertically excited tank is similar to the standing waves observed in the fixed tank (Fig. 3) but for this magnitude of $\kappa_v$, irregular peaks and troughs are generated in time. For higher wave steepness, as the solution evolves in time, a discrepancy in phase-shift between the numerical model and the approximate solution is evident; the fully non-linear model predicts waves of slightly longer period than the approximate solution. Differences in amplitudes, of both peaks and troughs, can also be observed. It should be noted that for small non-linearities ($\varepsilon = 0.0014$), a grid size of $40 \times 40$ resulted in sufficient accuracy in comparison with the second-order approximation (Fig. 9 (a)). However, the steeper wave case ($\varepsilon = 0.288$) required a finer grid resolution of $40 \times 80$ (Fig. 9(d)). It was again found to be more effective in ensuring accuracy by increasing the mesh density in the vertical direction than by using higher resolution horizontally. The non-dimensionalised time is defined as $t^* = \omega_1 t$, and the non-dimensional time step is $\Delta t^* = \omega_1 \Delta t$ where $\omega_1$ is the fundamental first sloshing frequency in a fixed tank. A non-dimensional time step of 0.011 was used for the test case in the stable region for both the small and steep wave cases. Fig. 9(b) and (e) show the corresponding phase-plane

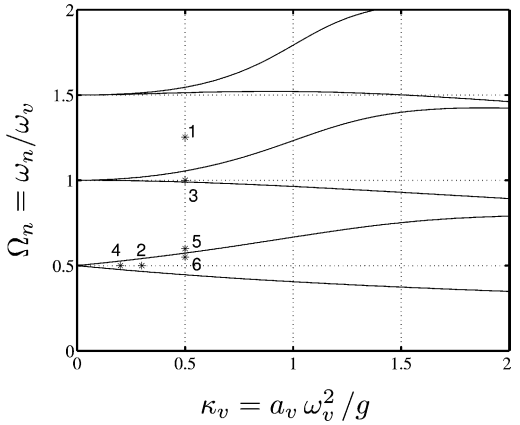


Fig. 8. Linear stability map of sloshing motion in vertically excited tank. Test cases (∗): (1) $\Omega_1 = 1.253$; $\kappa_v = 0.5$, (2) $\Omega_1 = 0.5$; $\kappa_v = 0.3$, (3) $\Omega_1 = 1.0$; $\kappa_v = 0.5$, (4) $\Omega_3 = 0.5$; $\kappa_v = 0.2$, (5) $\Omega_1 = 0.6$; $\kappa_v = 0.5$, (6) $\Omega_1 = 0.55$; $\kappa_v = 0.5$.

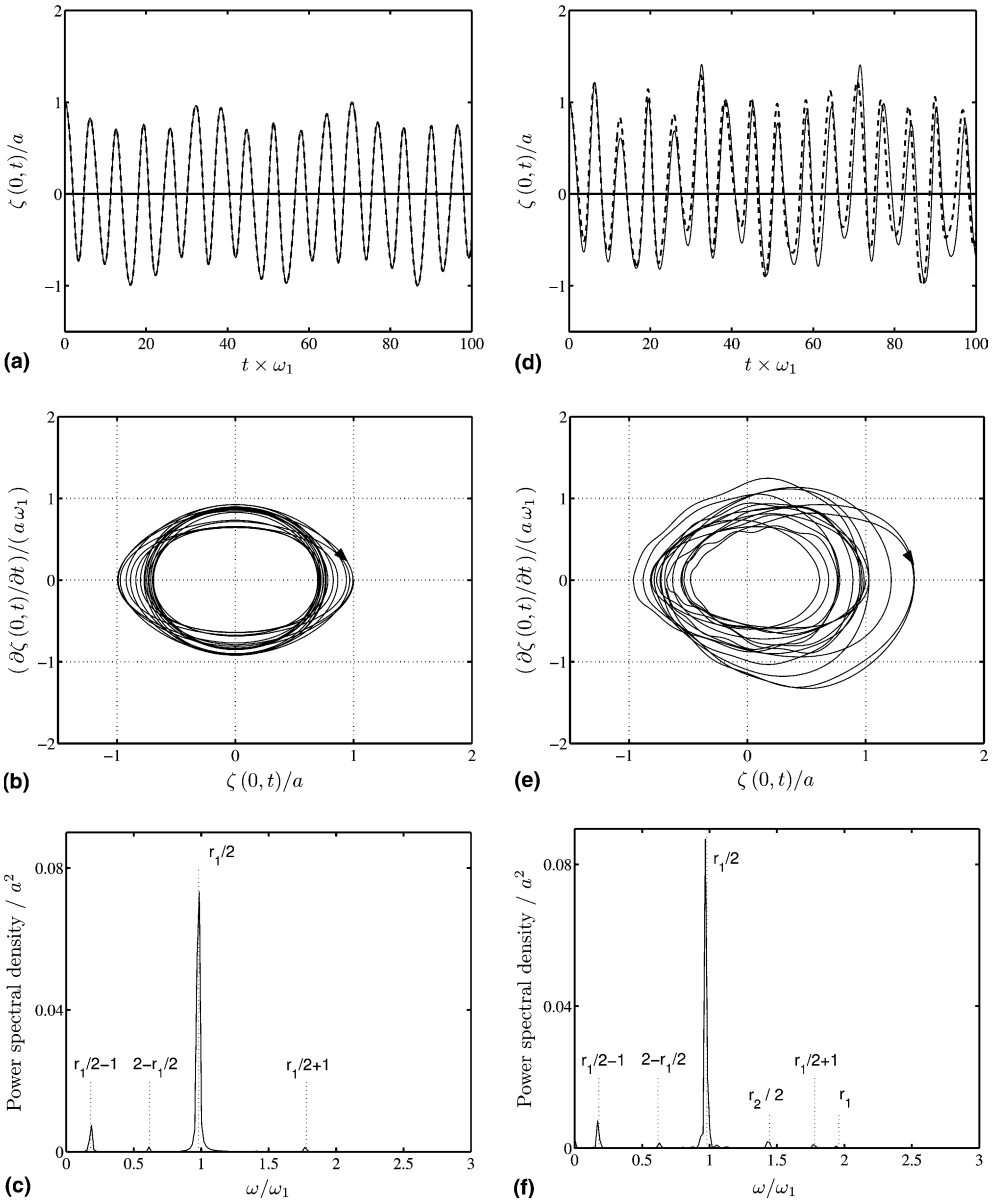


Fig. 9. Free-surface elevation at the left wall in vertically excited tank for $n = 1$ in stable region, $\Omega_1 = 1.253$, $\kappa_v = 0.5$ (Fig. 8: test case 1) for (a) $\varepsilon = 0.0014$ and (d) $\varepsilon = 0.288$. ---, second order solution; —, numerical solution. The corresponding wave phase-plane and spectra of the numerical model: (b, c) linear solution; (e, f) non-linear solution.

plots for the small and steep wave cases. The small amplitude wave phase-plane plot (b) displays linear behaviour of the free-surface through the closed orbit whereas the non-repeatable non-closed orbits of the large amplitude sloshing in (e) show that the free-surface exhibits more complicated behaviour typical of non-linear systems.

Fig. 9(c) and (f) shows the spectra corresponding to small and large amplitude wave cases (Fig. 9(a) and (d)). The linear solution (Fig. 9(c)) displays a dominating frequency of $r_1/2/\Omega_1$ near to the first fundamental

sloshing frequency ($\omega_1$) and secondary frequencies at $r_1/2 \pm 1/\Omega_1$. The non-linear solution (Fig. 9(f)) contains additional frequencies related to low energy content, including the second fundamental sloshing frequency ($r_2/2/\Omega_1$), which contributes to the non-linear generated waves.

Fig. 10 shows the free surface elevation time histories in unstable regions. The wave steepness parameter was kept constant at a low value of $\varepsilon = 0.0014$ and a grid size of $40 \times 40$ was used. A non-dimensional time

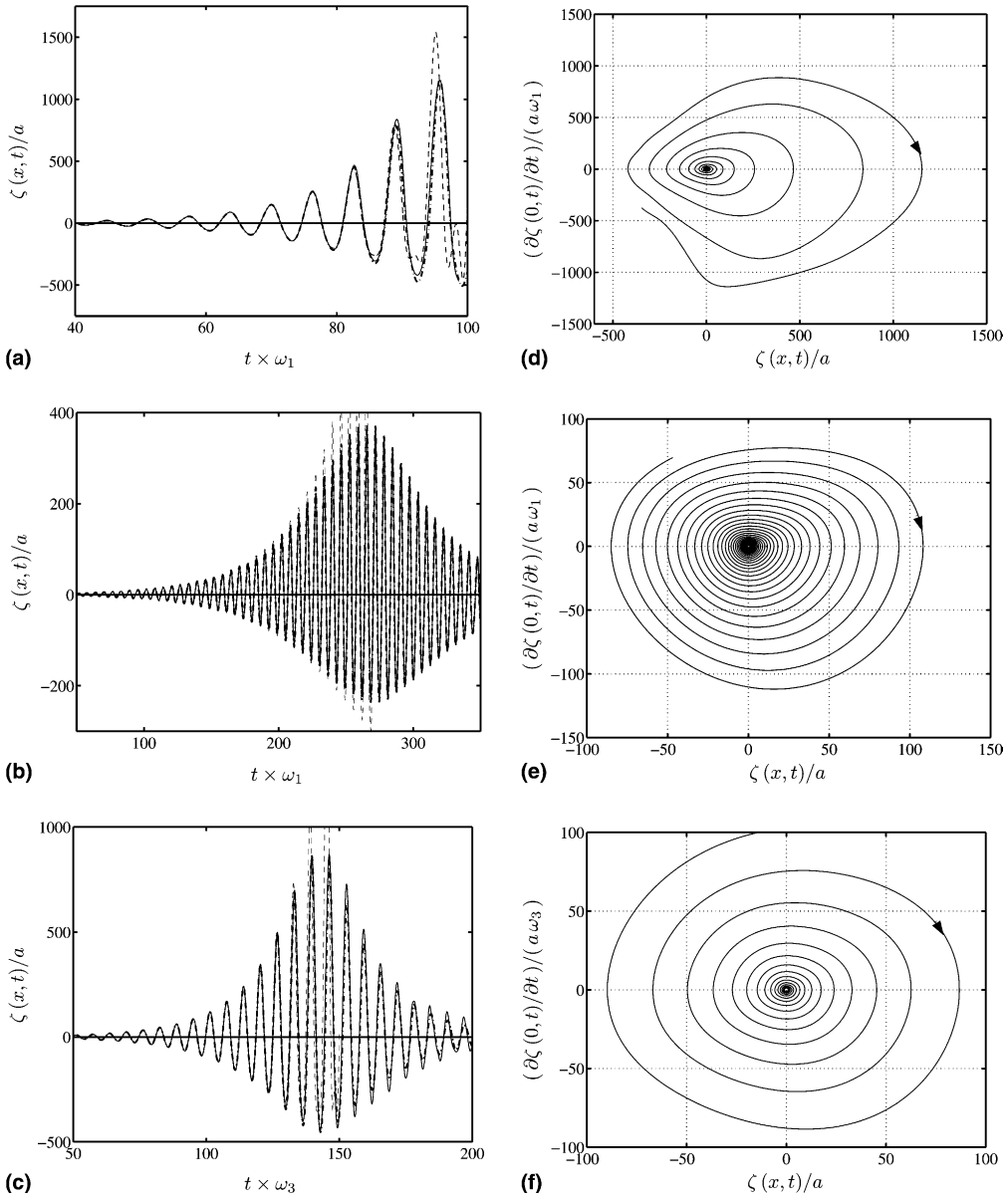


Fig. 10. Free-surface elevation at the left wall of vertically excited tank in unstable regions for small initial amplitude ($\varepsilon = 0.0014$): (a) $\Omega_1 = 0.5$, $\kappa_v = 0.3$ (Fig. 8: test case 2); (b) $\Omega_1 = 1.0$, $\kappa_v = 0.5$ (Fig. 8: test case 3); (c) $\Omega_3 = 0.5$, $\kappa_v = 0.2$ (Fig. 8: test case 4). - - -, second order solution; - · - · -, third order solution; —, numerical solution. The corresponding phase plots for the numerical model (d, e, f).

step of 0.011 was prescribed. Fig. 10(a) shows the free surface elevation time history for $\Omega_1 = 0.5$, $\kappa_v = 0.3$. The test, no. 2 in Fig. 8, corresponds to a first sloshing mode in the first instability region. From $t^* = 0$ to approximately 80, the wave amplitudes and phase predicted by the fully non-linear model are found to be in close agreement with the second order solution (26). Then the amplitudes begin to grow rapidly, discrepancies in amplitudes and phase between the numerical model and the second order solution increases, due to the enhanced non-linearity of the free surface motions. The third-order approximation (Section 3) compares almost exact with the numerical solution. However, the third-order solution predicts slightly deeper troughs and lower peaks as time evolves. The associated numerical predicted phase-plane diagram is shown in Fig. 10(d). Fig. 10(b) shows the free surface elevation time history $\Omega_1 = 1.0$, $\kappa_v = 0.5$ (test case 3 in Fig. 8). Following parameters were assumed: $\varepsilon = 0.0014$, $\Delta t^* = 0.011$ and a grid size of $40 \times 40$ was used. This is also an example related to the first sloshing mode but this particular free surface test case lies in the second instability region. As expected, the amplitudes do not grow rapidly in this region compared to the first instability region (Fig. 10(a)). We observe that the second order solution deviates from the numerical solution as times evolves whereas there is almost an exact agreement with the third order solution. Further we observe that the amplitude of the first mode start to grow in a resonance mode. As the amplitude increases the natural frequency changes. The change of the natural frequency with amplitude creates low frequency amplitude oscillations. This non-linear detuning effect is also in agreement with the numerical solution. Similar free-surface behaviour has also been observed by others, e.g., Hill [21]. Fig. 10(c) correspond to the third test case ($\Omega_3 = 0.5$, $\kappa_v = 0.2$, $\varepsilon = 0.0014$, $\Delta t^* = 0.020$ and grid: $40 \times 40$) which represents the second fundamental sloshing mode and lies in the first instability region (test case 4 in Fig. 8). Because it is a second mode, again the amplitudes are not found to grow rapidly in comparison with the first mode case (Fig. 10(a)). Again the second order solution deviates in peaks, troughs and phase compared to the numerical solution. The third order and the numerical solutions agree well, capturing the detuning effect. There is almost exact in-phase behaviour at all times. The peaks of the third order solution compare well with the numerical solution from $t^* = 0$ to approximately 150 at which time the amplitudes decays into a lower oscillation mode. Then the third order solution underestimate the peaks and troughs. Moreover, it can be observed in the associated numerical predicted phase-plane diagrams (Fig. 10(e) and (f)) that the free surface exhibits standard linear behaviour for an unstable system.

The final test of pure vertical tank excitation is carried out near the stability boundary (inside and outside). Test 5 in Fig. 8 represents a free surface problem which is just outside the instability region. Test 6 contains a set of parameters close to the ones of test case 5, but is located just inside the instability region. In Fig. 11 the free-surface elevation is simulated for small and steep amplitudes for these two cases. Although

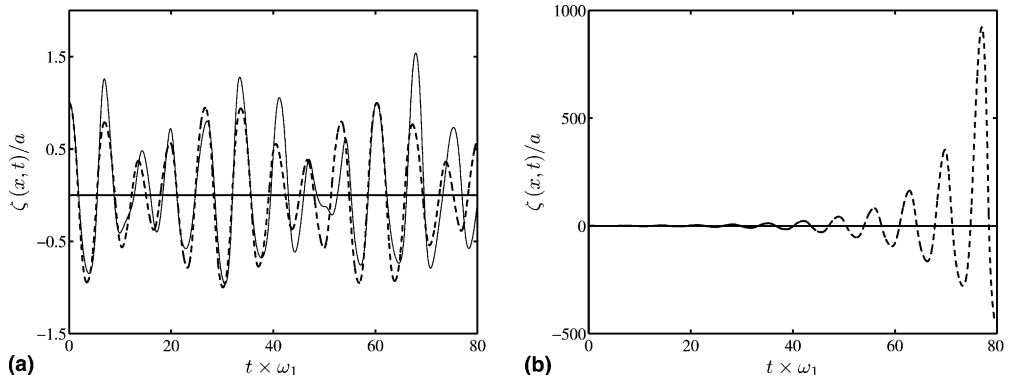


Fig. 11. Free-surface elevation at the left wall of vertically excited tank near stability boundary. (a) $\Omega_1 = 0.6$; $\kappa_v = 0.5$ – stable region (test case 5); (b) $\Omega_1 = 0.55$; $\kappa_v = 0.5$ – unstable region (test case 6). - - -, small initial amplitude ($\varepsilon = 0.0014$); —, large initial amplitude ($\varepsilon = 0.288$).

test case 5 and 6 have closely spaced parameters, the simulations of the numerical model illustrate the expected stable solutions for $\Omega_1 = 0.6$, $\kappa_v = 0.5$ and unstable solutions for $\Omega_1 = 0.55$, $\kappa_v = 0.5$. It is observed that the solution of test case 5 remains stable for both small and large initial wave steepnesses whereas the small initial wave steepness of test case 6 is sufficient to demonstrate a rapidly unstable solution.

## 7. Horizontally excited tanks

Investigations of forced sloshing of liquid in a rectangular 2-D tank subjected to horizontal base-excitation is undertaken in this section. The only change to the governing Eqs. (20)–(23) is the dynamical free-surface boundary condition (22) in which $Z''_T = 0$.

A linear solution for fluid motions with surface tension in a horizontally base-excited tank was first obtained by Faltinsen [10]. Herein surface tension is assumed to be negligible. We prescribe harmonic forced motion of $X_T(t) = a_h \cos(\omega_h t)$ where $a_h$ denotes the horizontal forcing amplitude, $t$ is time and $\omega_h$ is the angular frequency of forced horizontal motion. The initial conditions are $\phi_n^{(1,2)}(0) = 0$, $\zeta_n^{(1,2)}(0) = 0$, corresponding to the fluid being at rest. We use the coordinate system with $x$-axis fixed on the undisturbed water surface and $z$-axis fixed on the left-hand wall of the tank. The numerical predictions of the free surface motions in the horizontally excited tanks will be compared with analytical results from second- and third-order potential theory. When $\omega_v = 0$, it can be shown that the entire second order solution for the free-surface elevation and velocity potential can be written explicitly as

$$\zeta(x,t) = a_h \left( \sum_{n=0}^{\infty} \cos(k_n x) Z_n^{(1)}(\omega_h t) + \left( \frac{a_h \omega_h^2}{g} \right) \sum_{n=0}^{\infty} \cos(k_n x) Z_n^{(2)}(\omega_h t) \right) \tag{27}$$

and

$$\phi(x,z,t) = \frac{a_h g}{\omega_h} \left( \sum_{n=0}^{\infty} \frac{\cosh(k_n(z+h_s))}{\cosh(k_n h_s)} \cos(k_n x) \Phi_n^{(1)}(\omega_h t) + \left( \frac{a_h \omega_h^2}{g} \right) \sum_{n=0}^{\infty} \frac{\cosh(k_n(z+h_s))}{\cosh(k_n h_s)} \cos(k_n x) \Phi_n^{(2)}(\omega_h t) \right), \tag{28}$$

where $Z_n^{(2)}$ and $\Phi_n^{(2)}$ are

$$\begin{aligned} Z_n^{(2)'}(\omega_h t) - \Omega_n^2 \Phi_n^{(2)}(\omega_h t) &= \frac{1}{B^2} \left( C_n(K_n^2 \Phi_n^{(1)}, Z_n^{(1)}) - S_n(K_n \Phi_n^{(1)}, K_n Z_n^{(1)}) \right); \\ \Phi_n^{(2)'}(\omega_h t) + Z_n^{(2)}(\omega_h t) &= -\frac{1}{2B^2} S_n(K_n \Phi_n^{(1)}, K_n \Phi_n^{(1)}) - \frac{1}{2} C_n(\Omega_n^2 \Phi_n^{(1)}, \Omega_n^2 \Phi_n^{(1)}) - C_n(\Omega_n^2 \Phi_n^{(1)'}, Z_n^{(1)}), \end{aligned} \tag{29}$$

where $K_n = \pi n$ are non-dimensional wave numbers. It can also be shown that the first order solution reduces to

$$Z_n^{(1)'}(\omega_h t) - \Omega_n^2 \Phi_n^{(1)}(\omega_h t) = 0;$$

$$\Phi_n^{(1)'}(\omega_h t) + Z_n^{(1)}(\omega_h t) = -BB_n H''(\omega_h t).$$

The free surface motions are numerically examined off- and at resonance where resonance is occurring when the external horizontal forcing frequency ($\omega_h$) is equal to the natural sloshing frequency ($\omega_n$) of the liquid. The free-surface behaviour is investigated by varying the external force through the parameter $\kappa_h = a_h \omega_h^2 / g$ which is a measure of non-linearity. The results presented are for a tank of aspect ratio

$h_s/b = 0.5$, except for a special comparison study near the critical water depth (shown in the last part of this section).

Fig. 12(a) and (d) show the free-surface elevation at the left wall in an off-resonance region with $\omega_h/\omega_1 = 0.7$ for small horizontal forcing amplitude where $\kappa_h = 0.0036$ (a), and for large horizontal forcing amplitude where $\kappa_h = 0.036$ (d). The time histories of the forced sloshing analyses are non-dimensionalised

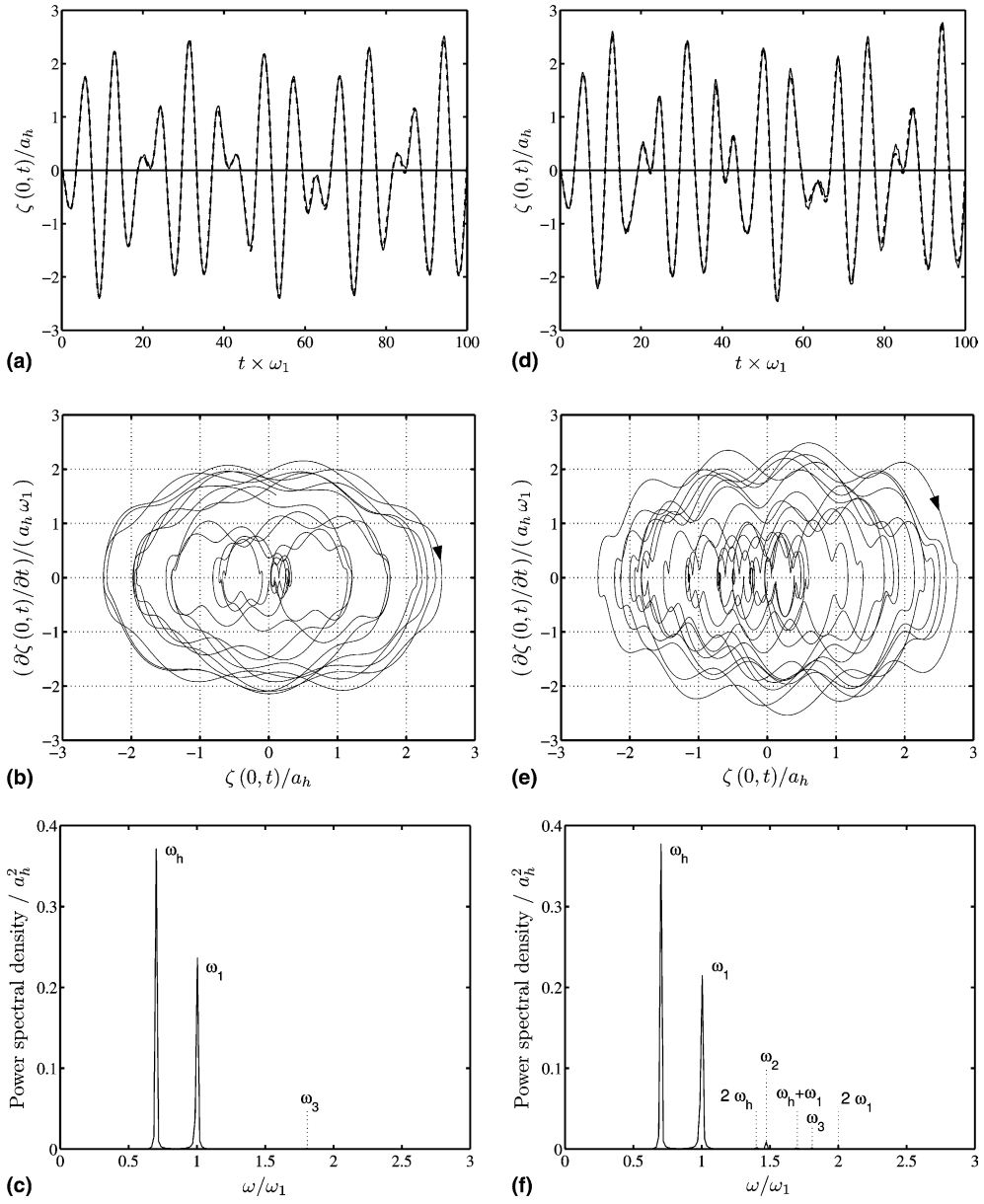


Fig. 12. Free-surface elevation at the left wall in horizontally excited tank; $\omega_h/\omega_1 = 0.7$; (a) $\kappa_h = 0.0036$ and (d) $\kappa_h = 0.036$; - - -, second order solution; —, numerical solution. The corresponding wave phase-plane and spectra of the numerical model: (b, c) linear solution; (e, f) non-linear solution.

with the first natural sloshing frequency. A grid size of $40 \times 40$ and $40 \times 80$, respectively, were prescribed for small and large forcing frequency. A time step of 0.003 s was used in both cases. Good agreement with the second order solution is achieved for both the case of small and large forcing frequency. The associated wave phase-planes (Fig. 12(b) and (e)) display linear behaviour of the free-surface with irregular patterns for the peaks and troughs in bounded orbits. Fig. 12(c) and (f) shows the associated spectra of the free surface elevation. It can be observed for the small forcing amplitude case (c) that there exists energy at two distinct frequencies, i.e. at the forcing frequency and at the first sloshing frequency. In addition, for the larger forcing amplitude case (f), a third frequency with low energy content exists ($\omega_2$) due to non-linear effects. This second natural sloshing frequency is responsible for the deviation between the numerical model and second order approximation.

The test case presented in Fig. 13 is also an off-resonance case but with a forcing frequency higher than the first natural sloshing frequency ($\omega_h/\omega_1 = 1.3$). As shown in the small amplitude spectrum (c) an additional (third) natural sloshing frequency is present in the solution of this particular free-surface problem. The free-surface time elevation for small amplitude waves ($\kappa_h = 0.0036$) is shown Fig. 13(a). Although $\omega_3$ has a low energy content it contributes to the lower numerical predicted peaks compared to the second order solution. The associated wave phase diagram (b) displays irregular peaks and troughs in bounded orbits. Next, the horizontal forcing parameter was increased to $\kappa_h = 0.072$ and the free-surface elevation simulated (Fig. 13(d)). The increase of $\kappa_h$ introduces non-linearity in the solution resulting in discrepancy in amplitudes between the fully non-linear model and the second order solution. As time evolves the phase between numerical model and approximate solution deviates, the numerical model having a longer period. This is due to the present of two additional secondary frequencies ($\omega_h \pm \omega_1$), as shown in the spectrum (f), which are generated by non-linear interaction between modes. For this reason the wave phase-plane (e) displays more irregular patterns compared to the small forcing frequency case (b).

Fig. 14 compares the small and large amplitude cases of the fully non-linear model for $\omega_h/\omega_1 = 0.7$ and 1.3. For stronger excitation it can be observed that the peaks are higher, the troughs are less deep and the period is longer than those of the approximate solution, which is typical non-linear effects.

Fig. 15 shows the free-surface elevation at the left wall at resonance, $\omega_h = \omega_1 = 3.76$ rad/s, for (a) small $\kappa_h = 0.0014$ and (c) large $\kappa_h = 0.014$ horizontal forcing amplitudes. For the small amplitude case there is good agreement between the approximate solutions and the numerical model. For the large amplitude case, at the initial stage of the process ($t\omega_1 < 20$) while the amplitude is still small, the numerical solution coincides with both the second-order and the third-order solutions. Eventually, as the amplitude increases, the non-linear effects begin to play a considerable role leading to higher peaks and smaller troughs in the surface elevation, compared to the third-order solution. As in the previous test cases the third-order solution predict the phase almost in exact agreement with the numerical solution. The second order solution do capture these non-linear features but discrepancy in amplitude and phase compared to the fully non-linear model is evident. This process can be observed even more clearly on the numerical predicted wave phase-planes, when the spiral trajectory of the linear solution (b) deforms gradually from cycle to cycle in the non-linear case (d), as the centre of the trajectory gradually moves towards higher amplitudes. The maximum steepness shown for the resonant solution (Fig. 15(c)) can be estimated to be approximately 0.25, and as shown the numerical solution begins to deviate from the linear one as the steepness reaches about 0.1.

As mentioned in Section 1, other investigators have analysed horizontal tank motion. Herein we compare a specific test case previously done by Hill [21] and Faltinsen et al. [11]. Their tank was 1.73 m wide with a still water depth of 0.6 m. We define the wave length as $\lambda = 2b/n$ and denotes the critical depth as $h_c$. At the critical depth the response changes from a "hard-spring" to a "soft-spring". Gu et al. [20], Faltinsen [11], Waterhouse [41] found $h_c/\lambda = 0.583$ m or in general $h_c = 0.337 \times b$ for the first mode, respectively. Since $h_s$ is 0.6 m, this particular study is a near critical depth case. Fig. 16 represents an off-resonance case [11,21] with a forcing frequency higher than the first natural sloshing frequency ($\omega_h/\omega_1 = 1.283$), similar to

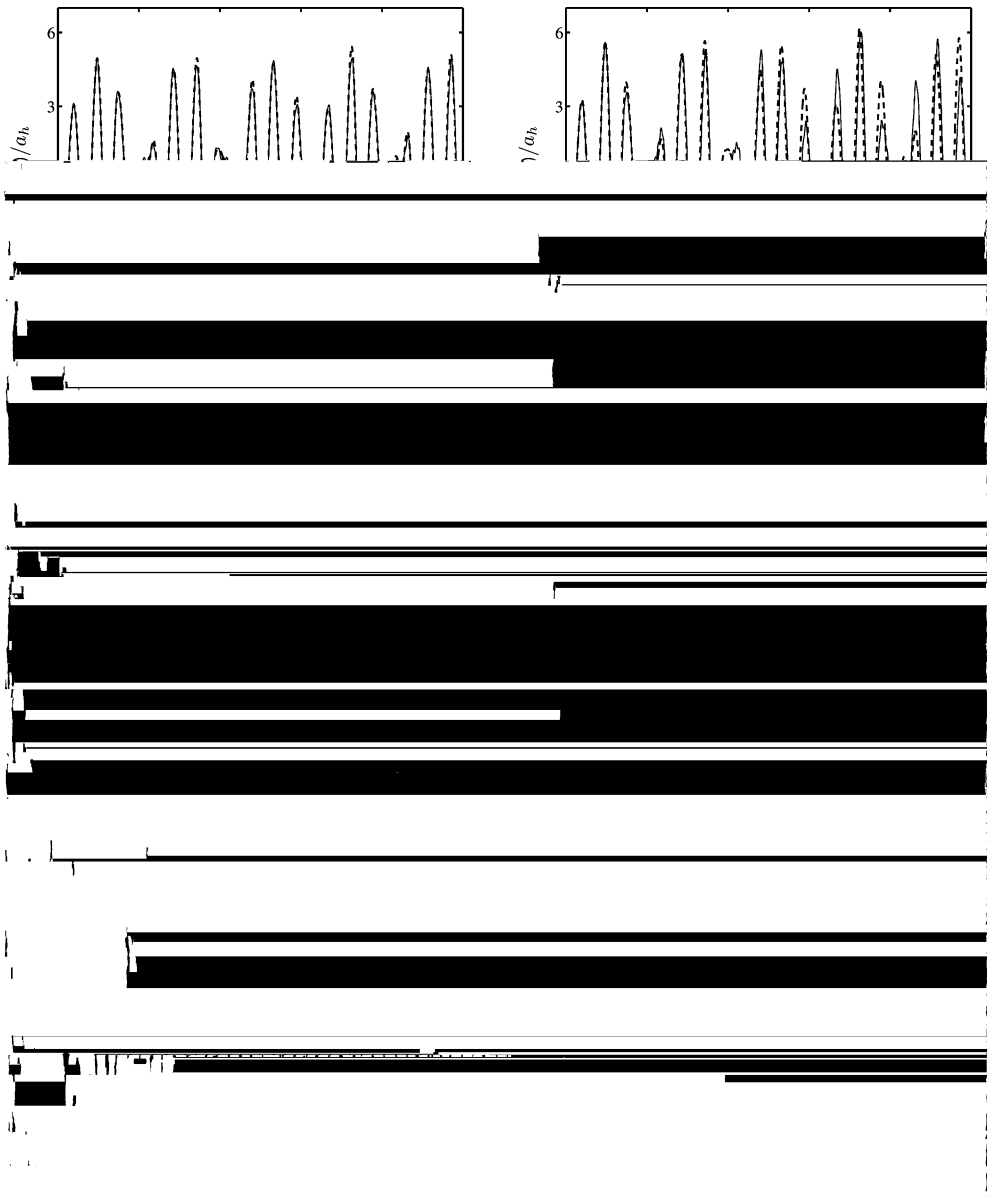


Fig. 13. Free-surface elevation at the left wall in horizontally excited tank; $\omega_h/\omega_1 = 1.3$; (a) $\kappa_h = 0.0036$ and (d) $\kappa_h = 0.072$; - - -, second order solution; —, numerical solution. The corresponding wave phase-plane and spectra of the numerical model: (b, c) linear solution; (e, f) non-linear solution.

Fig. 13 where $\kappa_h = 0.069$ (large). The fully non-linear solution (based on a grid size $40 \times 80$ and a time step of 0.003 s) is compared with Hill [21] who developed a third order solution assuming one dominating mode. We also compare with the second and third order solution (Section 3). The troughs of the third order solution compare well with the numerical results, as shown in Fig. 16. However the third order peaks are over estimated. The second order solution compare better with the numerical results than the third order, in the periods where the amplitudes are largest. The opposite is true for the smallest amplitudes. Hill's [21]

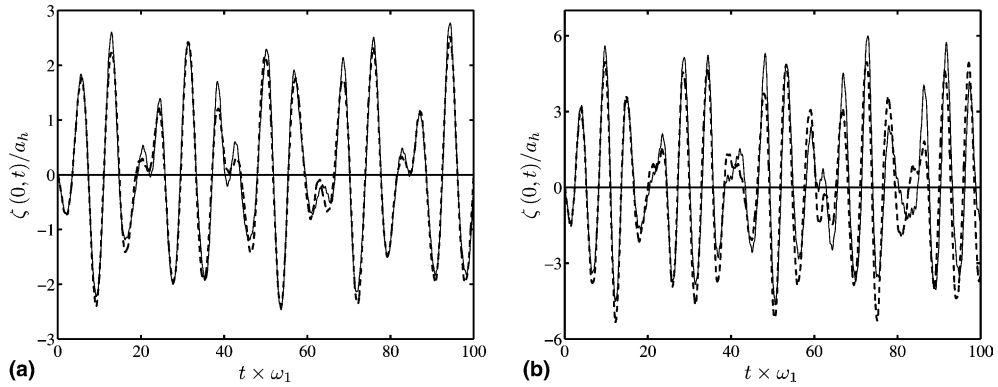


Fig. 14. Free-surface elevation at the left wall in horizontally excited tank. (a) $\omega_h/\omega_1 = 0.7$; - - -, small amplitude solution ($\kappa_h = 0.0036$); —, large amplitude solution ($\kappa_h = 0.036$). (b) $\omega_h/\omega_1 = 1.3$; - - -, small amplitude solution ($\kappa_h = 0.0036$); —, large amplitude solution ($\kappa_h = 0.072$).

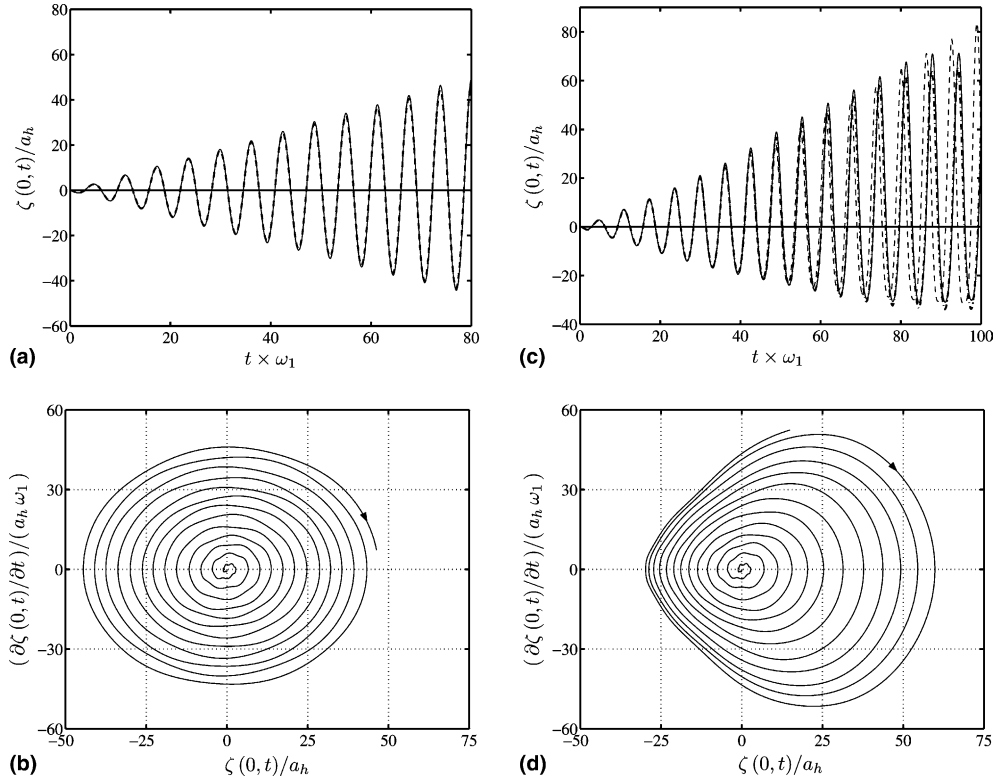


Fig. 15. Free-surface elevation at the left wall in horizontally excited tank at resonance; $\omega_h/\omega_1 = 1$; (a) $\kappa_h = 0.0014$ and (c) $\kappa_h = 0.014$; - · -, linear solution; - - -, second order solution; - · · -, third order solution; —, numerical solution. The corresponding phase-plane of the numerical model: (b) linear solution; (d) non-linear solution.

third order analytical-based algorithm generates a free surface elevation with smaller troughs/peaks compared to the fully non-linear solution. Also a phase shift is present compared to the other approximate solutions and the numerical method. Furthermore, Faltinsen et al. [11] did extensive theoretical and ex-

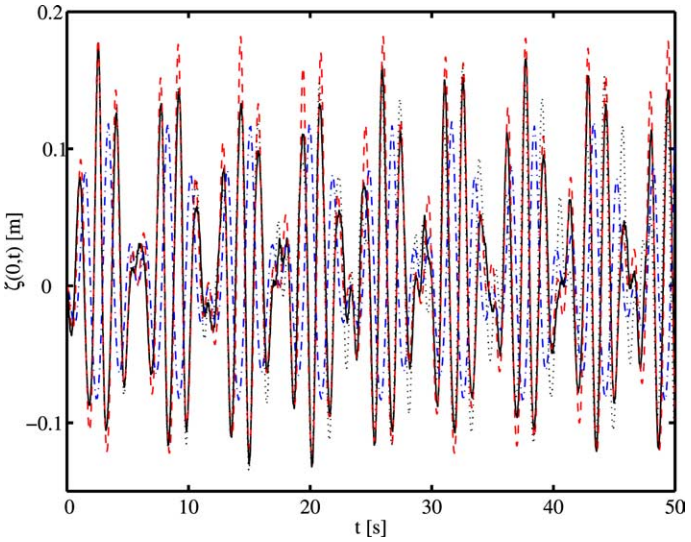


Fig. 16. Free-surface elevation at the left wall in horizontally excited tank; $\omega_h/\omega_1 = 1.283$; $a_h = 0.029$ m and $\kappa_h = 0.069$; —, numerical solution; ···, second order solution; - - -, third order solution; - · - ·, Hill (2003).

perimental sloshing experiments. Fig. 17 shows the theoretical result of Faltinsen et al. [11] of the above mentioned test case of Fig. 16. Their solutions generate peaks of 0.113 m/0.136 m and troughs of 0.107 m/0.1 m corresponding to the experimental and theoretical (impulse) tests. The present equivalent numerical solution generates 0.134 m/0.108 m at an equivalent time of 9.1 s/8.3 s, closer to the theoretical model. Later, as time evolves, at 37.1 s/37.8 s the numerical solution predicts peaks and troughs of 0.155 m/0.097 m. Faltinsen et al. predicts peaks/troughs of 0.127 m/0.087 m and 0.143 m/0.079 m corresponding to the experimental and theoretical (impulse) tests, respectively. Therefore the numerical solution is in reasonable agreement with the work of Faltinsen et al. for this particular test case.

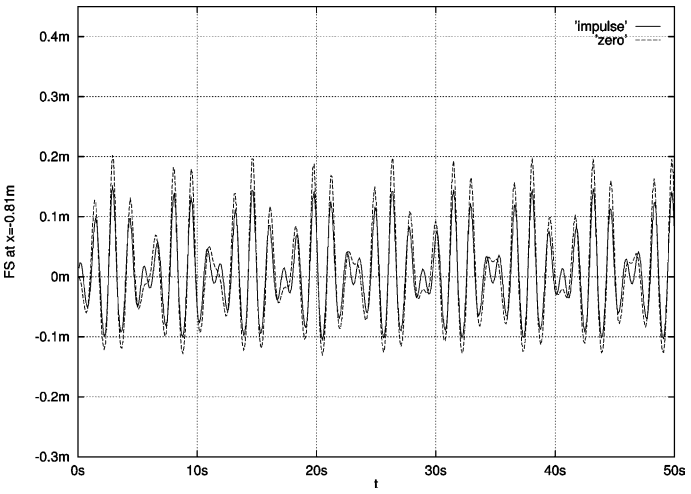


Fig. 17. Solution of Faltinsen et al. (2000) showing the free-surface elevation at the left wall in horizontally excited tank; $\omega_h/\omega_1 = 1.283$; $a_h = 0.029$ m and $\kappa_h = 0.069$. Theoretical predictions include two different initial conditions. The curve "Zero" corresponds to zero initial conditions, "Impulse" means initial impulse conditions.

## 8. Horizontally and vertically excited tanks

Let us now investigate the influence of vertical excitation on the solution for pure horizontal motion considered for $h_s/b = 0.5$ in the previous sections. As mentioned we use the general form of the excitation laws $X_T(t) = a_h H(\omega_h t)$; $Z_T(t) = a_v V(\omega_v t)$, where $a_{h,v}$, $\omega_{h,v}$ are the characteristic amplitudes and frequencies of horizontal and vertical motion, respectively. The initial conditions related to the fluid being at rest at time $t = 0$ are $\phi(x, z, 0) = 0, \zeta(x, 0) = 0$. We prescribe harmonic tank excitation in both horizontal and vertical directions with excitation law $V(\tau) = H(\tau) = \cos(\tau)$. In this case we can describe the individual sloshing modes in accordance with (11) which becomes unstable for certain values of parameters. It can be observed that the horizontal component of the motion generates perturbations with wave numbers $k_n$ corresponding to odd values of $n$ and $n = 0$. If any of the pairs of the parameters $(\Omega_n; \kappa_v)$, $n = 1, 3, \ldots$ lie in the instability region, then the corresponding mode grows in time exponentially. However, as we will demonstrate, if mode interaction occurs detuning effect may be present. The stability map of (11) is shown in Fig. 18. In the following, results are shown for the selected test cases with $k_v = 0.2, 0.3, 0.5$ including all associated individual sloshing modes, as marked in Fig. 18.

All models comprise $40 \times 40$ grid points for small horizontal forcing frequency and $40 \times 80$ grid points for large horizontal forcing frequency and a time step of 0.003 s. The tank dimensions and free sloshing frequencies are the same as in the previous sections ($h_s/b = 0.5$). The fully non-linear numerical results are compared with second-order and third-order approximate forms for standing waves in a tank moving in both horizontal and vertical directions. In the horizontally- and vertically-forced tank studies, the parameter $\kappa_h = a_h \omega_h^2/g$ is a measure of the importance of non-linearity. As mentioned, the equation for the combined motion (11) differs from the equation for pure vertical excitation, by the forcing terms due to the horizontal motion on its right hand side. These terms can produce resonance, which is recognised by the linear growth of the amplitude in time. Contrary to the pure horizontal motion we now have infinite number of resonances instead of one. Figs. 19–21 illustrate the time history of the free surface elevation at the left wall for three main resonant frequencies of the horizontal motion ($\omega_h/\omega_1 = 0.18$, 0.98, 1.78) in a

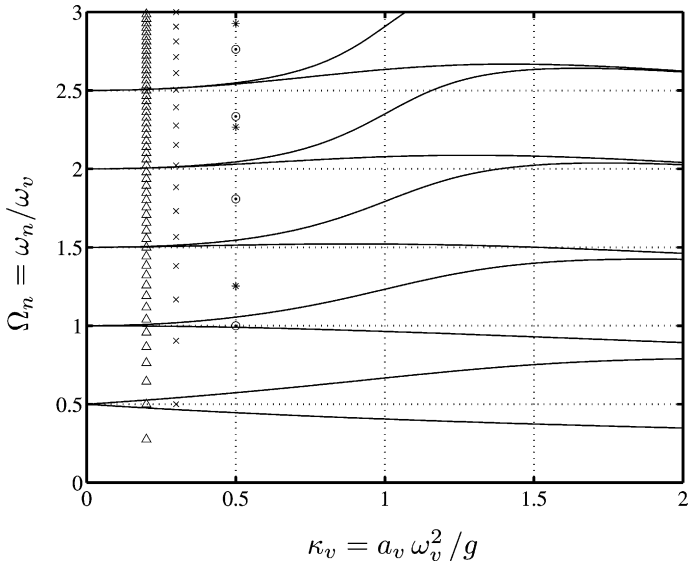


Fig. 18. Stability map for the first-order linear solution. Symbols represent points corresponding to the odd sloshing modes for selected cases. *: $\Omega_1 = 1.253$, $\kappa_v = 0.5$; ×: $\Omega_1 = 0.5$, $\kappa_v = 0.3$; ⊙: $\Omega_1 = 1.0$, $\kappa_v = 0.5$; △: $\Omega_1 = 0.276$, $\Omega_3 = 0.5$, $\kappa_v = 0.2$.

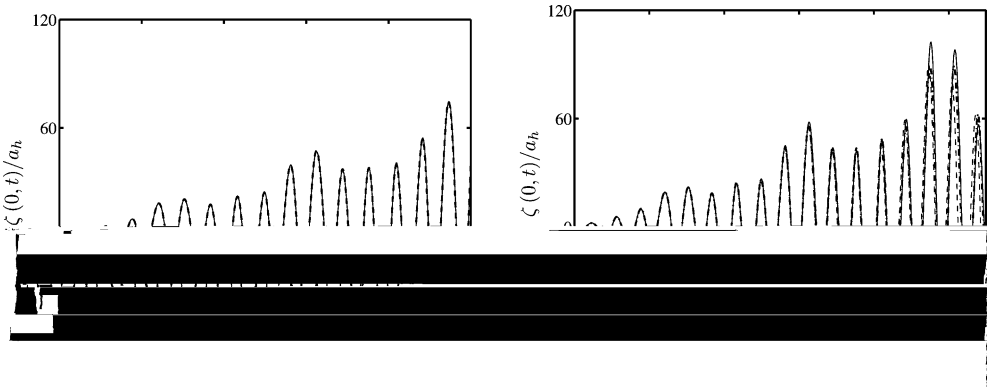


Fig. 19. Free-surface elevation at the left wall for the main resonances in horizontally and vertically excited tank $\Omega_1 = 1.253$, $\kappa_v = 0.5$, $\omega_h/\omega_1 = 0.98$. (a) $\kappa_h = 0.0014$ and (b) $\kappa_h = 0.0069$; - - -, second order solution; - - -, third order solution; —, numerical solution.

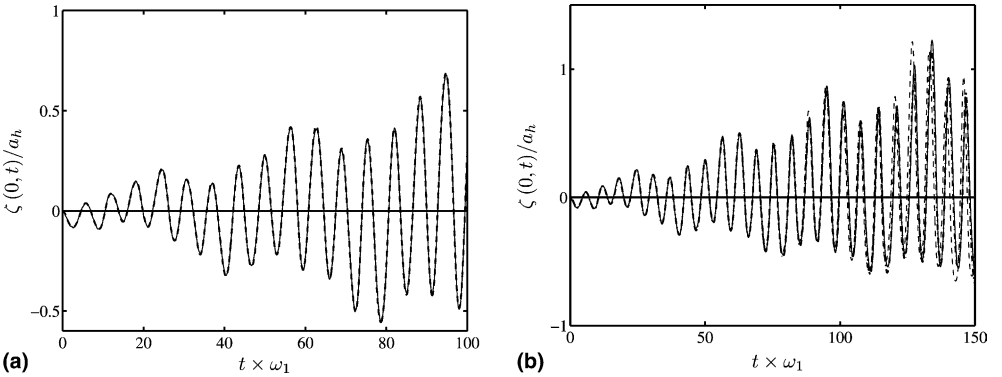


Fig. 20. Free-surface elevation at the left wall for the first side resonances in horizontally and vertically excited tank $\Omega_1 = 1.253$, $\kappa_v = 0.5$, $\omega_h/\omega_1 = 0.18$. (a) $\kappa_h = 4.85 \times 10^{-5}$ and (b) $\kappa_h = 0.0194$; - - -, second order solution; - - -, third order solution; —, numerical solution.

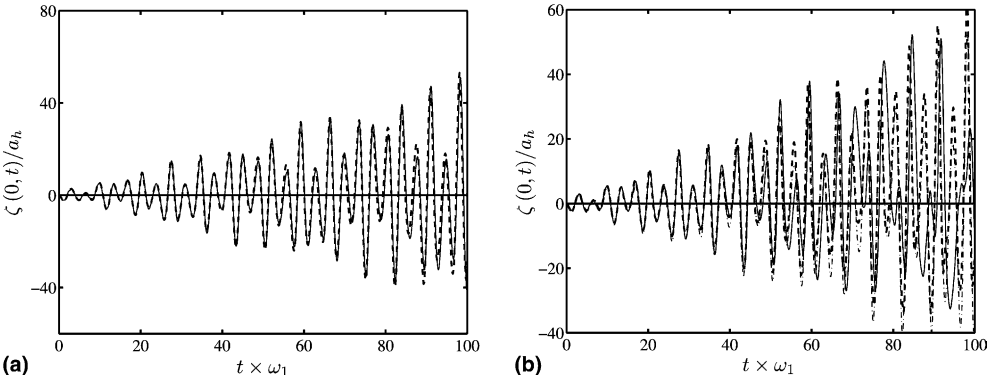


Fig. 21. Free-surface elevation at the left wall for the second side resonances in horizontally and vertically excited tank $\Omega_1 = 1.253$, $\kappa_v = 0.5$, $\omega_h/\omega_1 = 1.78$. (a) $\kappa_h = 0.0046$ and (b) $\kappa_h = 0.0228$; - - -, second order solution; - - -, third order solution; —, numerical solution.

stable region (first mode ($*$) in Fig. 18 or $r = 2.453$ in Fig. 1). The characteristics of the vertical tank motion are the same as in test case no. 1 in Fig. 8 ($\Omega_1 = 1.253$; $\kappa_v = 0.5$). The strongest of the resonant frequencies (Fig. 19) relate to the situation in which the horizontal forcing frequency is close to one of the free sloshing frequencies, here $\omega_1$. The two other resonant frequencies (Figs. 20 and 21) relate to the coupled frequencies ($\omega_v \pm \omega_h$) coinciding with a natural sloshing frequency. We note the resonance at the main frequency ($\omega_h/\omega_1 = 0.98$) is stronger and thus provides a higher rate of growth of perturbations compared to the secondary frequencies ($\omega_h/\omega_1 = 0.18, 1.78$), as can be observed by comparing the amplitudes in Figs. 19–21. For small horizontal forcing amplitude the numerical amplitude coincides with second-order small perturbation theory (Figs. 19(a) and 20(a)), and there is almost exact in-phase behaviour at all times. For higher horizontal forcing amplitude, the numerical non-linear solution is close to the approximate solutions from $t^* = 0$ to approximately 60, when the wave steepness is still small (Figs. 19(b) and 20(b)). The influence of non-linearity grows in time as the steepness increases, which can be observed by higher peaks and smaller troughs, which is the reason why the approximate solutions begin to deviate from the fully non-linear numerical model; the third-order being most accurate. The third resonant case, shown in Fig. 21, relates to the highest forcing frequency case ($\omega_h/\omega_1 = 1.78$) of the three selected tests. This high forcing frequency is responsible for the non-linearity produced at the free surface even for the small initial amplitude test shown in Fig. 21(a) ($\kappa_h = 0.0046$). Discrepancy between second/third-order and numerical solution in both amplitude and phase occurs as time evolves and becomes more pronounced for the large amplitude case ($\kappa_h = 0.0228$), as shown in Fig. 21(b). In general, we observe the free surface exhibits more complicated irregular behaviour than for pure horizontal excitation, due to the influence of vertical tank motion.

Fig. 22 shows the free surface elevation time histories and the associated wave phase diagrams for unstable solutions. These selected cases for $\kappa_v = 0.2, 0.3, 0.5$ are indicated in Fig. 18. The tests include a small horizontal forcing amplitude combined with the vertically excited tank cases (test no. 2, 3 and 4 in Fig. 8). The only difference when comparing the results of Fig. 22 with Fig. 10, is that the tank is moved horizontally with a small forcing amplitude. The free surface sloshing of the combined forced tank motion, shown in Fig. 22, illustrates that the instability is still due to the vertically forced motion and that the small horizontally forced tank motion only causes disturbance and delay in the occurrence of free surface instability. The free surface elevation of Fig. 22(a) represents the first sloshing mode in the first instability region (Fig. 18: $\times$: $\Omega_1 = 0.5, \kappa_v = 0.3$). From $t^* = 0$ to approximately 110, the wave amplitudes predicted by the fully non-linear model are found to be in close agreement with the second/third order solutions. Then the amplitudes begin to grow rapidly, discrepancies in amplitudes with the approximate solutions are found, as expected. The third-order solution is most accurate. The discrepancy is however minor because the first mode is dominating at all times. The associated wave phase diagram (Fig. 22(d)) displays more clearly the unstable system, showing the higher peaks and lower troughs as time evolves. Fig. 22(b) is an example of a first sloshing mode in the second instability region (Fig. 18: $\odot$: $\Omega_{1v} = 1.0$, $\kappa_v = 0.5$). This case therefore exhibit a less strong resonance than the test of Fig. 22(a). For this particular unstable system, the amplitudes are small for $t^* = 0$ to 200 and peaks and troughs have equal magnitude. The corresponding wave phase diagram (Fig. 22(e)) also shows the linear free surface behaviour. Therefore good agreement is found between the numerical model and the approximate solutions. The free surface behaviour shown in Fig. 22(c) has a stable first sloshing mode (Fig. 18: $\triangle$: $\Omega_{1v} = 0.276$, $\kappa_v = 0.2$). However, the third sloshing mode (Fig. 18: $\triangle$: $\Omega_{3v} = 0.5$, $\kappa_v = 0.2$) is an unstable solution in the first instability region. Therefore the entire solution becomes unstable. The amplitudes grow faster compared to the test of Fig. 22(b) because the solution is within the first instability region but is less in magnitude than the strong resonance case of Fig. 22(a), as expected. The numerical amplitudes and phase (c) deviate from both second-order and third-order solutions. The detuning effect of the third order solution is however well predicted in the sense that the third order non-linearity for the third mode is captured (note that the second-order solution is invalid at this stage). The shift in the third order solution compared to the fully non-linear solution is due to the influence of the first mode on the initial oscillations, at a time where the third mode has not started to grow.

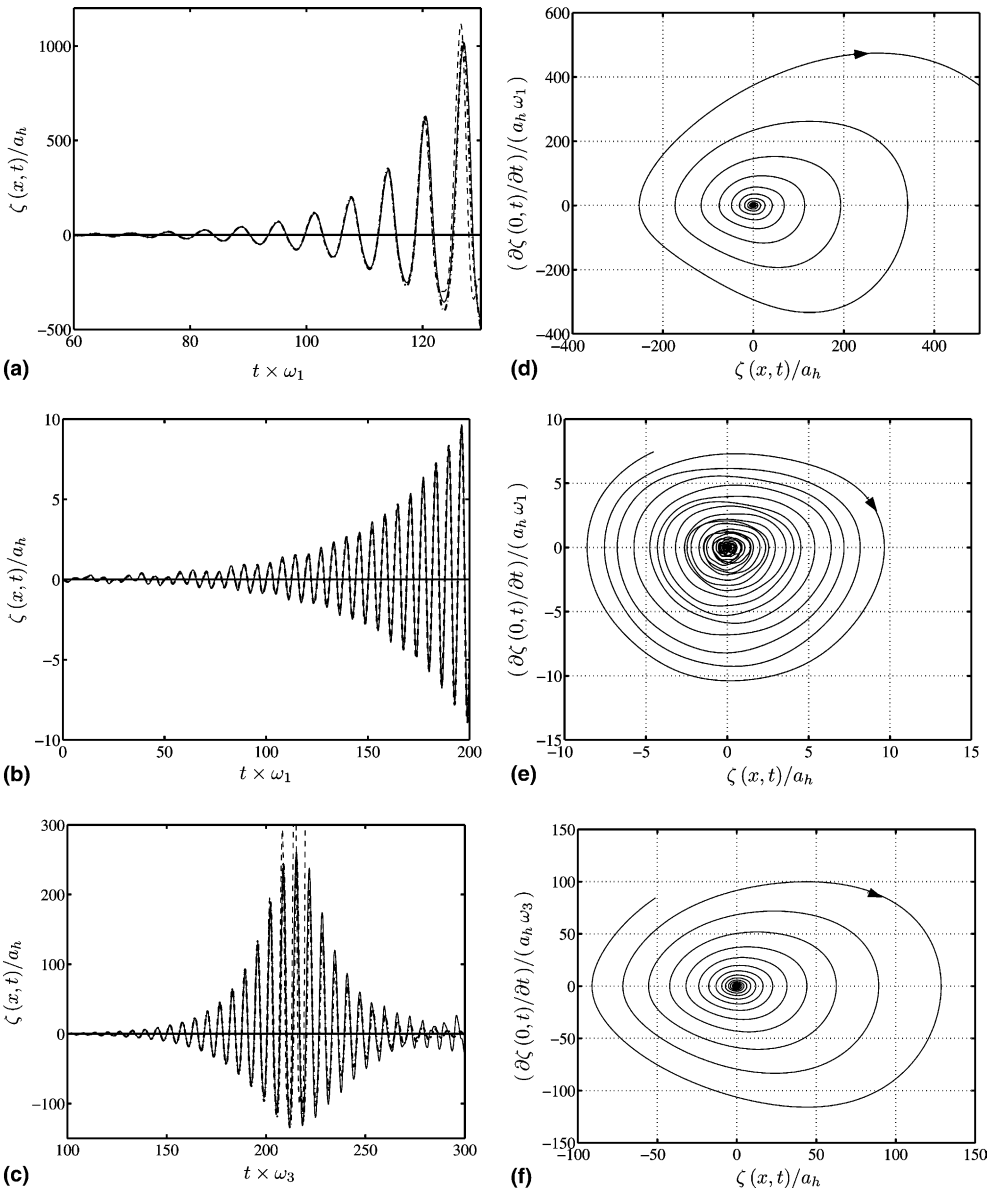


Fig. 22. Free-surface elevation at the left wall of horizontally and vertically excited tank for selected unstable cases (parametric resonance), - - -, second order solution; - - -, third order solution; —, numerical solution for small horizontal forcing ($a_h = 0.001$ m). (a) $\kappa_v, \Omega_1 = 0.3, 0.5$ (Fig. 18: $\times$); (b) $\kappa_v, \Omega_1 = 0.5, 1.0$ (Fig. 18: $\odot$); (c) $\kappa_v = 0.2$, $\Omega_{1v} = 0.276$, $\Omega_3 = 0.5$ (Fig. 18: $\triangle$). The associate wave phase diagrams of the numerical model (d, e, f).

The first–third mode interaction produces perturbations in the third mode which are predicted fairly well by the third order method (Section 3). However, multimodal algorithms [11] are recommended to be used in this case. For the corresponding vertical case (Fig. 10(c)), where the first mode is not excited, the agreement between third order and numerical solutions are better. The fully non-linear numerical predictions are also illustrated on the corresponding phase-plane plot (f).

Furthermore, we present the off-resonance case in a stable region for the horizontal motion ($\omega_h/\omega_1 = 0.7$) considered in the previous section (Fig. 12) coupled with a vertical motion at frequency $\omega_v = 3$ rad/s ($\Omega_1 = 1.253$) and vertical forcing parameter $\kappa_v = 0.5$ (Fig. 9). The horizontal forcing parameter is varied ($\kappa_h = 0.0036$, 0.036) representing small and large forced motion of $a_h = 0.01$, 0.1 m. With reference to the pure horizontal forced tank (Fig. 12) and the pure vertical forced tank motion (Fig. 9), the combined forced tank motion in Fig. 23 illustrates the change in the free-surface behaviour

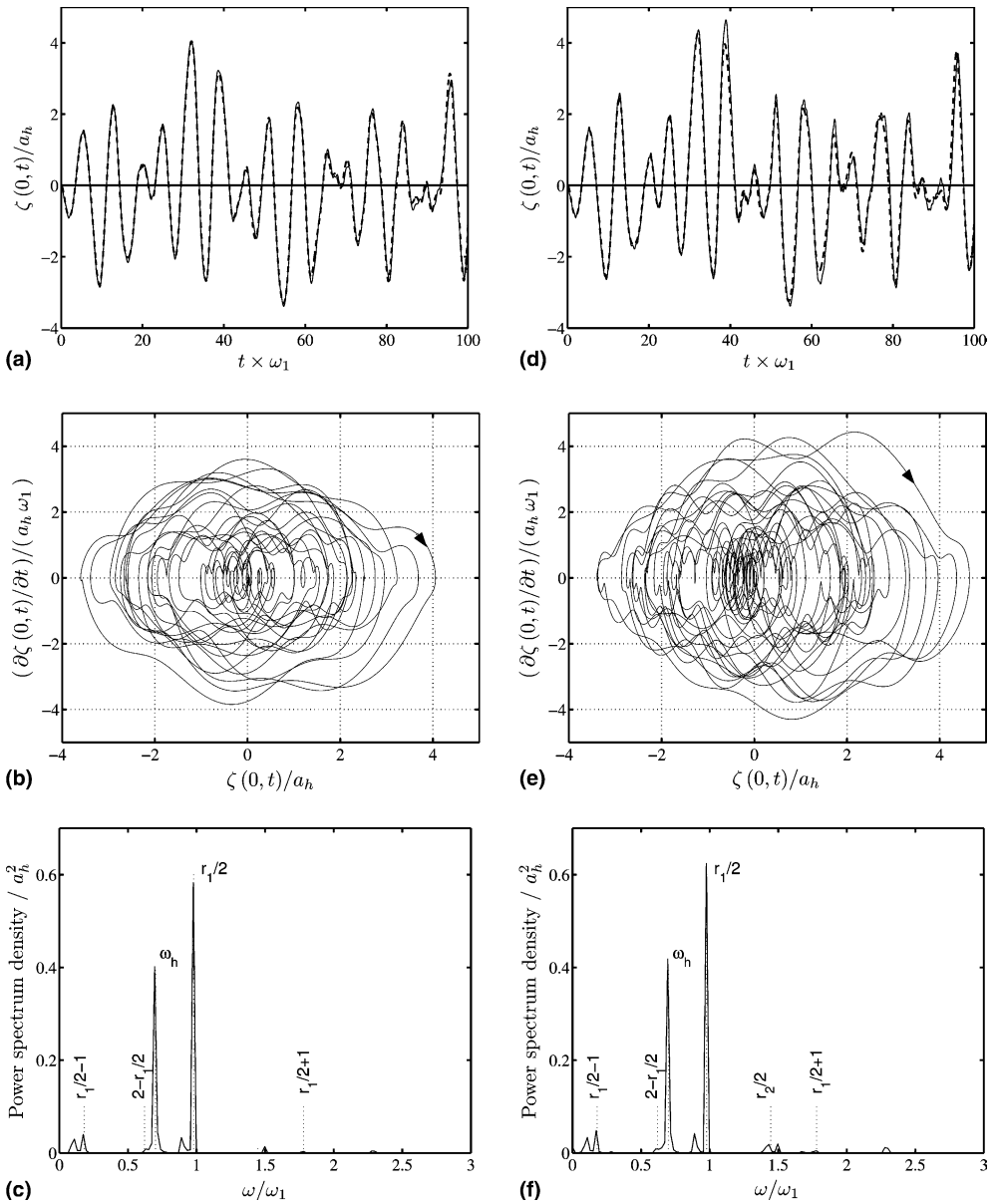


Fig. 23. Free-surface elevation at the left wall in horizontally and vertically excited tank; $\omega_h/\omega_1 = 0.7$; $\kappa_v = 0.5$; $\Omega_1 = 1.253$. (a) $\kappa_h = 0.0036$ and (d) $\kappa_h = 0.036$; - - -, second order solution; —, numerical solution. The corresponding wave phase-plane and spectra of the numerical model: (b, c) linear solution; (e, f) non-linear solution.

due to the vertical vibrations. The wave phase diagrams show more complicated surface elevation behaviour for both (b) linear and especially (e) non-linear solutions. The reason for this is the presence of additional frequencies in the spectrum due to the vertical motion, for example the coupled frequencies $\omega_v \pm \omega_h$. Figs. 23(c) and (f) show the spectra corresponding to the small and the large am-

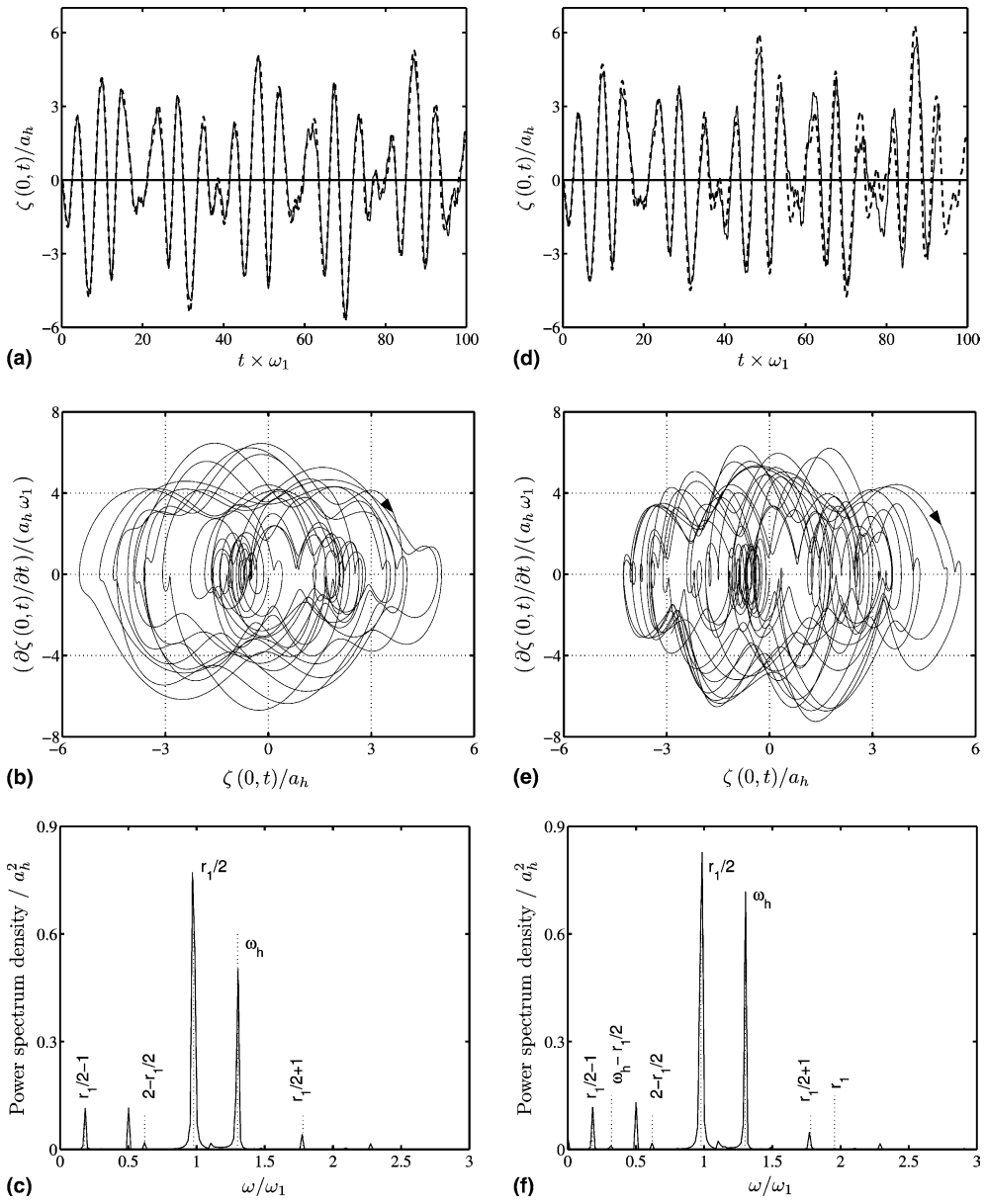


Fig. 24. Free-surface elevation at the left wall in horizontally and vertically excited tank; $\omega_h/\omega_1 = 1.3$; $\kappa_v = 0.5$; $\Omega_1 = 1.253$. (a) $\kappa_h = 0.0036$ and (d) $\kappa_h = 0.072$; - - -, second order solution; —, numerical solution. The corresponding wave phase-plane and spectra of the numerical model: (b, c) linear solution; (e, f) non-linear solution.

plitude wave cases (Fig. 23(a) and (d)). The linear solution (Fig. 23(c)) displays two dominating frequencies of which one is equivalent to the horizontal forcing frequency $\omega_h$ and the other $r_1/2/\Omega_1$ which is near the first natural sloshing frequency and secondary frequencies at $r_1/2 \pm 1/\Omega_1$. The non-linear solution (Fig. 23(f)) contains additional frequencies related to low energy content, including the second natural sloshing frequency ($r_2/2/\Omega_1$), which besides the large $\kappa_h$, contributes to the non-linear generated waves.

Next, as shown in Fig. 24, we explore another off-resonance case in the stable region which is similar to the previous mentioned test case (Fig. 13) but has an increased horizontal forcing frequency of $\omega_h/\omega_1 = 1.3$. We intend to investigate the effect of combining the forced horizontal tank test case of Fig. 13 and the vertically excited tank $\kappa_v = 0.5$; $\Omega_1 = 1.253$ (test case no. 1 in Fig. 8). As experienced in the pure horizontal case shown in Fig. 13(a)–(c) with small $\kappa_h$, non-linearity causes discrepancy in amplitudes as time evolves between the fully non-linear model and the second order solution even for small initial horizontally forced tank excitation (Fig. 24(a)). Irregular wave amplitudes are simulated with evidence of frequency coupling (double closely spaced peaks) between $\omega_h$ and $r_1/2/\Omega_1$ at approximately every $\Delta t^*$ of 20. Especially at these periods, the second order solution deviates from the fully non-linear model. Again the combined forced tank motion with a prescribed small forcing frequency contains secondary frequencies at $r_1/2 \pm 1/\Omega_1$. This was also found for the pure horizontally forced excited tank (Fig. 9(c)). The discrepancy between numerical model and second order solution grows when the horizontal forcing frequency is increased to $\kappa_h = 0.072$, as expected, when the non-linear parameter becomes larger. The non-linear effect is shown in Fig. 24(d)–(f). An additional frequency exists ($\omega_h - r_1/2$) compared to the small $\kappa_h$ test due to non-linear mode to mode interaction, as it can be observed for the larger amplitude of horizontal motion. Although the mode has a low energy content, as shown in Fig. 24(f), it is responsible for the deviation between the approximate form and the numerical model. The second order solution is incapable of capturing this non-linear effect. We note the non-linear effects will become enhanced if $\omega_h, \omega_1$ and $\omega_v$ become more closely spaced.

With reference to the pure horizontal forced tank motion shown in Fig. 14, Fig. 25 compares the small and the large combined tank motion with the frequency ratio of (a) $\omega_h/\omega_1 = 0.7$ and (b) $\omega_h/\omega_1 = 1.3$ for $\kappa_v = 0.5$; $\Omega_1 = 1.253$. The large amplitude solution deviates from the small amplitude solution in both peaks, troughs and phase. The effect is more pronounced for the high frequency case Fig. 14(b).

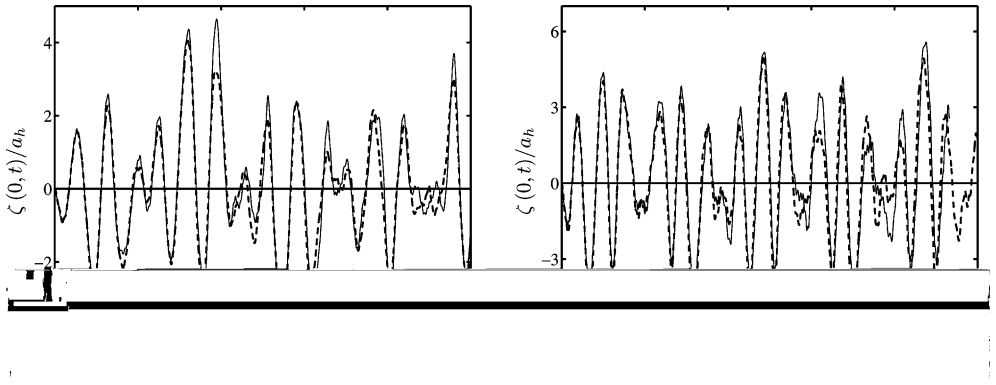


Fig. 25. Free-surface elevation at the left wall in a horizontally and vertically excited tank; $\kappa_v = 0.5$; $\Omega_1 = 1.253$. (a) $\omega_h/\omega_1 = 0.7$; - - -, small amplitude solution ($\kappa_h = 0.0036$); —, large amplitude solution ($\kappa_h = 0.036$). (b) $\omega_h/\omega_1 = 1.3$; - - -, small amplitude solution ($\kappa_h = 0.0036$); —, large amplitude solution ($\kappa_h = 0.072$).

## 9. Conclusions

Non-linear effects of standing wave motion of liquid in 2-D fixed and forced excited tanks have been investigated numerically. A fully non-linear inviscid numerical model has been developed based on potential flow theory with the mapped governing equations solved using finite differences.

Results of liquid sloshing induced by harmonic base excitations are presented for small to steep non-breaking waves. The simulations are limited to a single water depth above the critical depth corresponding to a tank aspect ratio of $h_s/b = 0.5$. We note that the numerical model is valid for any water depth except for small depth when viscous effects would become important. Moreover, solutions are limited to steep non-overturning waves.

First, simulations of sloshing motion in fixed tanks were carried out. The model was validated for different wave lengths and steepnesses. Good agreement between second order potential theory and the numerical model has been obtained for small amplitude wave cases. The numerical model captures high order non-linearities for the steep sloshing cases which was reflected by higher peaks, lower troughs and period elongation in comparison with second order potential theory. These are typical non-linear effects. It was found that the third-order single modal solutions compare in general well with the fully non-linear numerical predictions with almost exact agreement in phase at all times.

Second, sloshing motion in vertically excited tanks were carried out for stable and unstable solutions. Sloshing effects in a vertically excited tank in stable regions display similar behaviour to free sloshing motions in a fixed tank when the forcing parameter, $\kappa_v$, is small. This confirms the periodic behaviour of the small amplitude solution. When $\kappa_v$ grows, the fluid behaviour is no longer perfectly periodic, and so non-regular amplitudes result, even for the case of small amplitude waves. Non-linear effects complicate the fluid behaviour further, making it almost unpredictable. However, in stable regions, the solution remains bounded at all times. Vertical motions produce drastic effects within the instability regions, where parametric resonance takes place. In these regions, even small excitations can cause the growth of small initial perturbations, if the forcing acts on the tank for a sufficiently long time. We also demonstrate examples when the frequency changes during growing amplitudes (detuning effects). Good agreement between the third-order and numerical solution is found for the single mode dominant cases. We also showed that the second-order solution do not capture detuning effects.

Third, analyses were carried out with pure horizontal forced excitation including excitation frequencies off-resonance, and at resonant frequencies. The resonance in this case occurs at one of the natural sloshing frequencies. For the large forcing frequency, the third-order solution compares well with the numerical prediction. This is especially true with regard to the phase. The peaks were slightly underpredicted and the troughs slightly overestimated compared to the numerical results. Then, vertical forced vibrations were added and it was found that they significantly effect the resulting combined motion. In the unstable regions vertical excitation caused fast exponential growth of the waves generated by the small horizontal tank motion. Some of the test cases showed evidence of detuning effects. For example, a resonance mode changing into a low frequency mode of oscillations. It was shown that the discrepancy between third-order and numerical solution was minor for single dominant modes. Although detuning effect can be captured by the third-order solution, it was found that it does not work so well when modes interact. A multimodal algorithm should be used [11]. The combined motion test cases revealed results lying within the first and second instability regions showing a free-surface elevation with the highest growth rate of perturbations in the first region. It was also found that in addition to the resonant frequency of the pure horizontal excitation, an infinite number of additional resonance frequencies exist due to the combined motion of the tank.

In summary, it was demonstrated that the fully non-linear model provides solutions not obtainable with the approximate forms. This is especially true for steep waves, high forcing frequency and mode interaction cases. Each solution was obtained for both small and large amplitudes of horizontal or vertical or combined excitation in a tank with still water height of 1 m and tank length of 2 m. In general, the small-amplitude

free-surface predictions compare well with second-order theory, however, the numerical wave tank captures steep waves generated by large horizontal forcing amplitudes which differ from the third-order approximation. The maximum value of steepness, which is the measure of the non-linearity of the solution, obtained during the calculations was 0.3. It was found that for the present problem the relatively high steepness of 0.1 leads to a solution being significantly non-linear. In all cases, high amplitude solutions produce higher peaks and smaller troughs than small amplitude linear solutions. Furthermore, non-linear interaction between individual sloshing modes were demonstrated by extra peaks in the power spectrum of surface elevation, which leads to complicated irregular behaviour of the free-surface. In general, the liquid sloshing motion exhibits complicated behaviour due to both the horizontal and vertical forced tank motion. It is shown that vertical excitation causes the instability associated with parametric resonance of the combined motion for a certain set of frequencies and amplitudes of the vertical motion while the horizontal motion is related to classical resonance.

The numerical model is simple, computationally quick and accurate. For the cases presented herein there was no need for free surface smoothing. The present potential flow model provides a simple way of simulating steep non-breaking waves, that may be readily extended to the prediction of 3-D wave motion.

## References

[1] M. Abramovitz, I.A. Stegun, Handbook of Mathematical Functions, Dover Publications, New York, 1972.
[2] H.N. Abramson, The dynamics of liquids in moving containers, Rep. SP 106, NASA, 1966.
[3] H.N. Abramson, R.L. Bass, O. Faltinsen, H.A. Olsen, Liquid slosh in lng carriers, in: 10th Symposium on Naval Hydrodynamics, Cambridge, Massachusetts, ACR-204, 1974, pp. 371–388.
[4] T.B. Benjamin, F. Ursell, The stability of the plane free surface of a liquid in a vertical periodic motion, Proc. R. Soc. Lond. Ser. A 225 (1954) 505–515.
[5] H. Bredmose, M. Brocchini, D.H. Peregrine, L. Thais, Experimental investigation and numerical modelling of steep forced water waves, J. Fluid Mech. 490 (2003) 217–249.
[6] A. Cariou, G. Casella, Liquid sloshing in ship tanks: a comparative study of numerical simulation, In Marine Struct. 12 (1999) 183–189.
[7] M.S. Celebi, H. Akyuldiz, Nonlinear modeling of liquid sloshing in moving rectangular tank, In Ocean Eng. 29 (2002) 1527–1553.
[8] W. Chen, M.A. Haroun, F. Liu, Large amplitude liquid sloshing in seismically excited tanks, Earthquake Eng. Struct. Dyn. 25 (1996) 653–669.
[9] M.J. Chern, A.G.L. Borthwick, R. Eatock Taylor, A pseudospectral $\sigma$-transformation model of 2-D nonlinear waves, J. Fluids Struct. 13 (1999) 607–630.
[10] O.M. Faltinsen, A nonlinear theory of sloshing in rectangular tanks, J. Ship Res. 18 (4) (1974) 224–241.
[11] O.M. Faltinsen, O.F. Rognebakke, I.A. Lukovsky, A.N. Timokha, Multidimensional modal analysis of nonlinear sloshing in a rectangular tank with finite water depth, J. Fluid Mech. 407 (2000) 201–234.
[12] O.M. Faltinsen, O.F. Rognebakke, A.N. Timokha, Resonant three-dimensional nonlinear sloshing in a square-base basin, J. Fluid Mech. 487 (2003) 1–42.
[13] O.M. Faltinsen, A.M. Timokha, Asymptotic modal approximation of nonlinear resonant sloshing in a rectangular tank with small fluid depth, J. Fluid Mech. 470 (2002) 319–357.
[14] M. Faraday, On a peculiar class of acoustical figures, and on certain forms assumed by groups of particles upon vibrating elastic surfaces, Phil. Trans. R. Soc. Lond. 121 (1831) 299–340.
[15] P. Ferrant, D. Le Touze, Simulation of sloshing waves in a 3D tank based on a pseudo-spectral method, in: Proc. 16th International Workshop on Water Waves and Floating Bodies, Hiroshima, Japan, 2001.
[16] J.B. Frandsen, A.G.L. Borthwick, Simulation of sloshing motions in fixed and vertically excited containers using a 2-D inviscid $\sigma$-transformed finite difference solver, J. Fluids Struct. 18 (2) (2003) 197–214.
[17] J. Gerrits, Dynamics of liquid-filled spacecraft, PhD thesis, Rijks Universiteit Groningen, Holland, 2001.
[18] D.M. Greaves, A.G.L. Borthwick, G.X. Wu, R. Eatock Taylor, A moving boundary finite element method for fully non-linear wave simulations, J. Ship Res. 41 (3) (1997) 181–194.
[19] X.M. Gu, P.R. Sethna, Resonance surface waves and chaotic phenomena, J. Fluid Mech. 183 (1987) 543–565.
[20] X.M. Gu, P.R. Sethna, A. Narain, On three-dimensional nonlinear subharmonic resonance surface waves in a fluid: part i – Theory, J. Appl. Mech. 55 (1988) 213–219.
[21] D.F. Hill, Transient and steady-state amplitudes of forced waves in rectangular basins, Phys. Fluids 15 (6) (2003) 1576–1587.

[22] C.W. Hirt, B.D. Nichols, Volume of fluid (vof) method for the dynamics of free boundaries, J. Computat. Phys. 39 (1981) 201–225.
[23] R.A. Ibrahim, V.N. Pilipchuk, T. Ikeda, Recent advances in liquid sloshing dynamics, ASME Appl. Mech. Rev. 54 (2) (2001) 133–199.
[24] L. Jiang, M. Perlin, W.W. Schultz, Period tripling and energy dissipation of breaking standing waves, J. Fluid Mech. 369 (1998) 273–299.
[25] L. Jiang, C-L. Ting, M. Perlin, W.W. Schultz, Moderate and steep faraday waves: instabilities, modulation and temporal asymmetries, J. Fluid Mech. 329 (1996) 275–307.
[26] A. Kareem, T. Kijewski, Y. Tamura, Mitigation of motions of tall buildings with specific examples of recent applications, J. Wind Struct. 2 (3) (1999) 201–251.
[27] M.B. Kocygit, R.A. Falconer, B. Lin, Three-dimensional numerical modelling of free surface flows with non-hydrostatic pressure, Int. J. Numer. Meth. Fluids 40 (2002) 1145–1162.
[28] L.D. Landau, E.M. Lifshitz, Mechanics, third ed., Butterworth-Heinemann, London, 1976.
[29] G.L. Mellor, A.F. Blumberg, Modelling vertical and horizontal diffusivities with the sigma transform system, Appl. Ocean Res. 113 (1985) 1379–1383.
[30] J. Miles, D. Henderson, Parametrically forced surface waves, Ann. Rev. Fluid Mech. 22 (1990) 143–165.
[31] H. Ockendon, J.R. Ockendon, Resonant surface waves, J. Fluid Mech. 59 (1973) 397–413.
[32] M. Perlin, W.W. Schultz, Capillary effects on surface waves, Ann. Rev. Fluid Mech. 32 (2000) 241–274.
[33] N.A. Phillips, A coordinate system having some special advantages for numerical forecasting, J. Meteorol. 14 (1957) 184–185.
[34] I. Tadjbakhsh, J.B. Keller, Standing surface waves of finite amplitude, J. Fluid Mech. 8 (1960) 442–451.
[35] J.G. Telste, Calculation of fluid motion resulting from large amplitude forced heave motion of a two-dimensiomal cylinder in a free surface, in: Proceedings of the Fourth International Conference on numerical Ship Hydrodynamics, Washington, USA, 1985, pp. 81–93.
[36] C.-P. Tsai, D.-S. Jeng, Numerical Fourier solutions of standing waves in finite water depth, Appl. Ocean Res. 16 (1994) 185–193.
[37] M.S. Turnbull, A.G.L. Borthwick, R. Eatock Taylor, Numerical wave tank based on a $\sigma$-transformed finite element inviscid flow solver, Int. J. Numer. Meth. Fluids 42 (2003) 641–663.
[38] S. Ushijima, Three-dimensional arbitrary Lagrangian–Eulerian numerical prediction method for non-linear free surface oscillation, Int. J. Numer. Meth. Fluids 26 (1998) 605–623.
[39] J-M. Vanden-Broeck, L.W. Schwartz, Numerical calculation of standing waves in water of arbitrary uniform depth, Phys. Fluids 24 (5) (1981) 812–815.
[40] J.C. Virnig, A.S. Berman, P.R. Sethna, On three-dimensional nonlinear subharmonic resonance surface waves in a fluid: part ii – Experiment, J. Appl. Mech. 55 (1988) 220–224.
[41] D.D. Waterhouse, Resonance sloshing near critical depth, J. Fluid Mech. 281 (1994) 313–318.
[42] G.X. Wu, R. Eatock Taylor, Finite element analysis of two-dimensional non-linear transient water waves, Appl. Ocean Res. 16 (1994) 363–372.
[43] G.X. Wu, Q.A. Ma, R. Eatock Taylor, Numerical simulation of sloshing waves in a 3D tank based on a finite element method, Appl. Ocean Res. 20 (1998) 337–355.